

WRF Model Sensitivity to Choice of Parameterization: A Study of the 'York Flood 1999'

Renji Remesan¹, Tim Bellerby², Ian Holman¹, Lynne Frostick³

¹ Cranfield Water Science Institute, Cranfield University

² Department of Geography, Environment and Earth Science, University of Hull

³ Centre for Adaptive Science, University of Hull

Abstract:

Numerical weather modelling has gained considerable attention in the field of hydrology especially in un-gauged catchments and in conjunction with distributed models. As a consequence, the accuracy with which these models represent precipitation, sub-grid-scale processes and exceptional events has become of considerable concern to the hydrological community. This paper presents sensitivity analyses for the Weather Research Forecast (WRF) model with respect to the choice of physical parameterization schemes [both cumulus parameterisation (CPSs) and microphysics parameterization schemes (MPSs)] used to represent the '1999 York Flood' event, which occurred over North Yorkshire, UK, 1st -14th March 1999. The study assessed four CPSs [Kain–Fritsch (KF2); Betts–Miller–Janjic (BMJ); Grell–Devenyi ensemble (GD) and the old Kain–Fritsch (KF1)] and four MPSs [Kessler, Lin et al., WRF Single-Moment 3-class (WSM3) and WRF Single-Moment 5-class (WSM5)] with respect to their influence on modelled rainfall. The study suggests that the BMJ scheme may be a better cumulus parameterization choice for the study region, giving a consistently better performance than other three CPSs, though there are suggestions of underestimation. The WSM3 was identified as the best microphysics scheme and a combined WSM3/BMJ model setup produced realistic estimates of precipitation quantities for this exceptional flood event. This study analysed spatial variability in WRF performance through categorical indices including: POD, FBI, FAR and CSI during 'York Flood -1999' under various model settings. Moreover, the WRF model was good at predicting high intensity rare events over the Yorkshire region, suggesting it has potential for operational use.

Key words: numerical rainfall prediction; WRF, cumulus parameterization, microphysics York floods,

Corresponding Address:

Dr Renji Remesan

Cranfield Water Science Institute, Cranfield University

Vincent Building, Cranfield campus, MK43 0AL

E: r.remesan@cranfield.ac.uk

38 T: +44 (0)1234

39

40 **1. Introduction:**

41

42 Precipitation intensity, timing (onset timing and duration), spatial distribution of precipitation
43 in basin etc. have great importance in state-of-art operational hydrology, integrated flood
44 management approaches and advanced techniques to predict extreme hydrological events.
45 Climate variability and its implications on water resources and extreme flood events have
46 direct impacts on agriculture, road traffic, manufacturing and construction activities. Owing
47 to climate change and its possible effects on water resources, hydrologists are seeking
48 downscaling methods that can link atmospheric and hydrological models for hydrological
49 simulations with reliable accuracy (Kite and Haberlandt., 1999; Wood et al., 2004). High-
50 resolution global assimilated weather data from models such as the Weather Research and
51 Forecasting (WRF) mesoscale model are very important sources of information capable of
52 providing credible input data to modern regional hydrological models. Tang and Dennis
53 (2014) evaluated the capability of WRF with the Variable Infiltration Capacity (VIC)
54 hydrological model and highlighted good agreement in the simulation of monthly and daily
55 soil moisture, and monthly evaporation in the Upper Mississippi River Basin (UMRB) from
56 1980 to 2010. This study highlighted that results from offline linkage of model could be used
57 to reproduce certain climate variables and hydrological variables like soil moisture. Another
58 reanalysis data driven WRF study by Wenhua and Chung-Hsiung (2013) reproduced the
59 spatial distributions of daily mean precipitation and rainy days similar to that of Tropical
60 Rainfall Measuring Mission (TRMM) Multisatellite Precipitation Analysis 3B42 product data
61 in Western North Pacific. TRMM data are a widely acceptable global gridded data set among
62 the hydrological community. Such WRF success stories in various environmental and
63 geographic circumstances have accumulated knowledge and confidence in the hydrological
64 community to directly use high resolution WRF outputs in their hydrological models (e.g.
65 Liong et al 2013). In the meantime hydrologists are also interested in the sensitiveness in
66 precipitation and other meteorological variables with WRF model structure. One can find
67 several studies of two-way coupling of the operational mesoscale weather prediction model
68 with land surface hydrological models (Seuffert et al., 2002). Givati et al (2012) employed
69 the WRF model to provide precipitation forecasts to run an operational streamflow forecast
70 system for the Jordan River. Bugaets and Gonchukov (2014) have coupled WRF with Soil

71 and Water Assessment Tool (SWAT 2012) using OpenMI 2.0 and web-service technologies
72 and this integrated structure was used for real time hydrological modelling and forecasting
73

74 However, many publications have highlighted precipitation as one of the most difficult
75 variables to simulate in numerical weather models and regional climate models (Giorgi et al.,
76 1993; Zhang et al., 2003). A study by Pall and Eltahir (2001) has pointed out the difficulties
77 of explicitly simulating local variability of atmospheric variables like precipitation rates at
78 sub-grid scales in weather models. Therefore, many cumulus parameterization schemes
79 (CPSs) and micro physical schemes have been developed and implemented in numerical
80 weather prediction models to represent convective processes more effectively(e.g., Kuo
81 1974; Grell 1993). In a model, micro physical schemes mechanise processes controlling
82 formation of cloud droplets and ice crystals, their growth and fallout as precipitation;
83 whereas, the Cumulus convection plays a major role in the energetics and dynamics of
84 atmospheric circulation systems (Kuo, 1974). Most of these schemes are developed in
85 specific convective environments, so a systematic evaluation for the local climate of interest
86 here is essential to yield useful information that can assist hydrological modellers who are
87 specially working in catchment level (Ishak et. al., 2012). Seeing that many real-time floods
88 forecasting and river level warning systems use high resolution data from mesoscale
89 numerical models and couple these with state-of art- hydrological models, it is essential to
90 assess the prediction sensitivity of the various meteorological variables obtained from various
91 model configurations, scheme settings and diverse modelling resolutions. Many studies have
92 identified that the selection of parameterization and microphysical schemes is the main
93 reason for inconsistency of modelling and accuracy of predicted weather variables under
94 various convective environments (Kerkhoven et al. 2006).

95 The WRF model is a next-generation mesoscale numerical weather prediction system
96 designed in collaborative partnership, principally among the National Center for Atmospheric
97 Research (NCAR) and the National Oceanic and Atmospheric Administration. It is one of the
98 most sophisticated and widely accepted dynamic downscaling models in the literature for
99 precipitation prediction. Fowle and Roebber (2003) and Fritsch and Carbone (2004) have
100 highlighted the significance of cloud microphysics parameterizations in performance of the
101 WRF model in rainfall modelling. Krishnamurti et al. (1999) suggested that there appears to
102 be no single model that consistently gives best results, due not only to the chaotic nature of
103 the atmosphere but also due to limitations in the initial conditions of the model and

104 parameterisations. Ruiz and Saulo (2010) have used WRF over South America in different
105 configurations to identify the best configuration which gives reliable estimates of observed
106 surface variables. A number of sensitivity studies have considered the effects of different
107 parameterization schemes including Cumulus Parameterization Schemes (CPSs) and
108 microphysics parameterizations schemes (MPSs) (Hu et al 2010; Salimun et al 2010). Fovell
109 and Su (2007) show how cloud microphysical parameterization and convection details
110 significantly affect hurricane track forecasts at operational resolutions (30 and 12 km). They
111 compared the effects of the Kessler, Lin et al, and the three class WRF single moment
112 (WRF3) schemes, coupled with the effects of Kain-Fritsch (KF1), Grell-Devenyi (GD), and
113 Betts-Miller-Janjic (BMJ) convective parameterization schemes.

114 This paper considers the evaluation and optimisation of different CPSs and MPSs of the WRF
115 model with respect to the prediction of high intensity extreme events happening in the United
116 Kingdom. The study focused on the Yorkshire Upper Derwent catchment located in the
117 north east of England, which is consistently under flood risk. The Yorkshire Derwent
118 Catchment Flood Management Plan (CFMP) has undertaken significant work to reduce the
119 risk of flooding from the river especially following the March 1999 floods in the region. We
120 will refer to this flood event as the York Flood – 1999. Reliable hydro-atmospheric
121 conjunctive modelling systems play a significant role in the delivery of effective flood
122 forecasting, flood warning and emergency response services during extreme high intensity
123 precipitation events. The purpose of this study is to investigate the impact of WRF model
124 settings in cumulus and microphysics parameterization schemes and to provide insight into
125 the capabilities of modelling to reproduce rare storm events such as York flood - 1999. For
126 this purpose, we have conducted high resolution WRF model simulations of the
127 unprecedented rainfall events that occurred over the Yorkshire-Humber side region during
128 first half of March-1999, using ECMWF ERA – 40 data as boundary conditions. We
129 conducted rainfall simulations using several cumulus parameterization and microphysical
130 schemes at different resolutions and compared the results with available ground based data.
131 In this study, CPS sensitivity analysis was conducted using four schemes: Kain–Fritsch, KF2
132 (Kain 2004), Betts–Miller–Janjic, BMJ (Janjic 1994, 2000); Grell–Devenyi ensemble, GD
133 (Grell and Devenyi 2002); old Kain–Fritsch, KF1 (Kain and Fritsch 1990). Four
134 microphysics parameterization schemes (MPSs) were considered: Kessler (Kessler 1969);
135 Lin et al. (Lin et al. 1983), WRF Single-Moment 3-class, WSM3 (Hong et.al. 2004); WRF
136 Single-Moment 5-class, WSM5 (Hong et al., 2006). The study aimed to identify the best

137 schemes and WRF model settings to represent individual transient rare weather systems for
138 the Yorkshire-Humberside region and to reproduce the observed spatial variability and
139 statistics of precipitation extremes.

140 In the subsequent sections of this paper, the land based observed precipitation data sets from
141 the Yorkshire-Humberside region during York Flood -1999 and the WRF model setup are
142 summarized. A detailed statistical analysis of the model performance under different settings
143 of CPSs and MPSs against observations is presented in the results section. Finally, the
144 discussions and conclusions are given in the fourth section of the paper.

145 **2. Materials and Methods**

146 **2.1 Derwent and York Flood 1999**

147 Yorkshire-Humberside region has a wide network of Rivers like Aire, Don, Esk (and coastal
148 streams), Hull (and coastal streams), Ouse, Ribble and Tees alongside the River Derwent.
149 The Yorkshire-Humber region is a winter flood prone part of England due to interactions of
150 the major river network, significant storm rainfall in the catchments and substantial amount
151 of snowmelt contributions to the rivers. This study focussed on the upper Derwent catchment
152 extending over 1586 km², draining to Buttercrambe (UK Ordnance Survey Grid Reference
153 SE 731587) in North Yorkshire. At the source and in the upper regions, the major river and
154 its tributaries run over the Corallian limestone formation. The average annual rainfall in the
155 region is 779 mm, out of which approximately 59% is accounted for by evapotranspiration.
156 Annual rainfall over the northern half of the catchment (North York Moor) exceeds 1,000
157 mm in some years (Remesan, *et al.*, 2013).

158 The Derwent catchment has a long history of flooding with recorded evidence dating back to
159 1892. Prior to the heavy flooding in 1999, the previously highest recorded flood was in 1947
160 (Environment Agency, 2007). The catchment was particularly badly affected by flooding in
161 1927, 1930, 1931, 1932, 1947 and 1960 and in more recent times, during March 1999. In this
162 study we are focusing on the capabilities of WRF to predict the rainfall which occurred
163 during first two weeks of March which lead to the York flood - 1999. A low pressure fronts
164 moved east to west between February 28th and March 9th, bringing first snow, then rain, so
165 that melting snow added to the run-off. During 4-5th March 1999, exceptional levels of
166 rainfall were experienced in the Derwent catchment area, reaching 125 millimetres (4.9 in)
167 inside a 24 hour period. The situation was worsened by melting snow which had earlier

168 accumulated on the North York Moors. Church Houses in Farndale had over 302 mm (11.89
169 inches) of rain between 28th February and 11th March, and other stations recorded similar
170 figures (RNHS, 2013). In this study, simulated results obtained from WRF under different
171 model settings were compared with observed data during 1st – 14th March of 1999 from 22
172 selected stations in the region. Details of those stations are given in the Table 1. The rainfall
173 data observed at different points in the Derwent catchment are shown in Figure 2 and in a
174 cumulative form in the Figure 3.

175 **2.2 Weather Research and Forecasting (WRF) Model and Design of Experiments**

176 The Advanced Research WRF version 3.3 (WRF, cited 2013) is a new-generation mesoscale
177 modelling system (Skamarock et al., 2005) and successor of the well regarded MM5 model
178 that serves both operational and research communities. WRF is a nonhydrostatic, primitive-
179 equation, mesoscale meteorological model with advanced dynamics, physics and numerical
180 schemes. The current WRF software framework (WSF) supports two dynamical solvers: the
181 Advanced Research WRF (ARW) and the nonhydrostatic Mesoscale Model (NMM). These
182 two solvers accompany a dynamic core which includes mostly advection, pressure-gradients,
183 coriolis, buoyancy, filters, diffusion, and time-stepping. WRF possesses a number of
184 outstanding features including: 1. Incorporation of advanced numerics and data assimilation
185 techniques, 2. Multiple relocatable nesting capability, 3. Enhanced physics in treatment of
186 convection and mesoscale precipitation, 4. Better handling of topography than the Eta model,
187 5. Much less diffusive, larger effective resolution, permits longer time steps. 6. Allows real
188 data and idealized simulations in same framework, 7. Plug-in architecture, moving nests and
189 nudging. These capabilities enable the model for a wide range of applications, from idealized
190 research to operational forecasting, with priority given to horizontal grids of 1–10 kilometers.
191 The WRF model uses terrain-following, hydrostatic-pressure vertical coordinates with the top
192 of the model being a constant pressure surface. There are numerous physics options in the
193 WRF model, the major details about its configuration in this study is shown in the Table 2.
194 As shown in the Table 2, different physical parameterisations (e.g.: boundary layer, the
195 convection and radiation schemes) including the Yonsei University scheme for the planetary
196 boundary layer (Hong et al., 2006), the Dudhia shortwave radiation scheme (Dudhia, 1989),
197 the rapid radiative transfer model for long-wave radiation scheme and Pleim-Xiu Land
198 Surface Model have been used.

199 WRF is a mesoscale regional model that requires climatic data, generated by any global
200 model, at its lateral boundaries to drive the model. In this study, the European Centre for
201 Medium-Range Weather Forecasts (ECMWF), ERA-40 data set was used to drive it. Many
202 sources of meteorological observations were used, including radiosondes, balloons, aircraft,
203 buoys, satellites, and scatterometers over more than 40-years. The model initial and lateral
204 boundary conditions are derived from the ECMWF 40-year reanalysis (ERA-40) data with
205 the improved resolution of $1^{\circ} \times 1^{\circ}$ and updated every 6 hour. The four nested domain
206 dimensions of the WRF simulations for the Yorkshire-Humberside region are shown in
207 Figure 1. The simulations of all selections of CPSs and MPSs were performed on a nested
208 domain with the child domains [d02 (9 km), d03 (3km) and d04 (1km)] and parent domain
209 [d01 (27 km)] as shown in figure 1. The four domains are centred over the Upper Derwent
210 catchment with domain sizes of $918 \times 756 \text{ km}^2$, $495 \times 522 \text{ km}^2$, $246 \times 255 \text{ km}^2$ and 103×94
211 km^2 for d04, d03, d02 and d01 respectively. Details of the grid spacing, grid number and the
212 downscaling ratio of the experiments are given in Table 3. This study has performed
213 simulations for each selection of CPSs and MPSs for 1176 hours (2 weeks) starting at 00.00
214 UTC 01st March 1999 and finishing at 00.00 UTC 15th March 1999. A total of 8 simulations
215 were conducted using four different CPSs of the WRF model [KF1, KF2, BMJ and GD] and
216 another four MPSs [Kessler, Lin et al scheme, WSM3 and WSM5]. Some details of different
217 CPSs are given in Table 4. The resolution of the innermost domain was fixed with a
218 horizontal grid spacing of 1 km. The time steps of the four domains, which also govern the
219 time intervals of the output rainfall series, are set to 3 hrs, 1 hr, 1 hr and 1hr, respectively
220 from the outermost to the innermost domain. However, here we have presented a comparison
221 of daily temporal and spatial simulation results because of availability of good quality land
222 based daily data from 22 weather stations.

223

224 **2.3 Verification Methods for WRF Simulations**

225 Both categorical and the continuous indices have been employed as statistical measures for
226 the spatial and temporal verification of meteorological model outputs against land-based
227 rain gauge data (Stanski et al., 1989; Jolliffe and Stephenson, 2003; Wilks, 2006; Liu et al.,
228 2012). The most commonly used categorical verification indices are the probability of
229 detection (POD), frequency bias index (FBI), false alarm ratio (FAR) and the critical success
230 index (CSI). The POD index gives an idea of the fraction of the observed precipitation that is

231 correctly predicted by the model; this index ranges from 0 to 1, with 1 being a perfect score,
 232 and it is sensitive to the frequency of rainfall occurrence during the event. FBI gives an
 233 indication of overestimation or underestimation but it is also sensitive to how well
 234 precipitation simulations match observed values. The FBI ranges from 0 to ∞ with 1
 235 indicating a perfect match. CSI ranges between 0 and 1 and this index specifies how the
 236 simulated precipitation corresponds to the observed precipitation. This index is a popular
 237 categorical verification index in numerical weather modelling. It is sensitive to ‘hits’ and
 238 penalises both ‘misses’ and ‘false alarms’ but does not distinguish sources of simulation
 239 error. FAR quantifies the fraction of the simulated rainfall that did not actually occur. This
 240 indicator ignores ‘misses’ and it is also sensitive to the frequency of precipitation occurrence
 241 during the event. The equations for these categorical indices are given below:

$$242 \quad POD = \frac{1}{n} \sum_{i=1}^n \frac{PP_i}{PP_i + NP_i} \quad (1)$$

$$243 \quad FBI = \frac{1}{n} \sum_{i=1}^n \frac{PP_i + PN_i}{PP_i + NP_i} \quad (2)$$

$$244 \quad FAR = \frac{1}{n} \sum_{i=1}^n \frac{PN_i}{PP_i + PN_i} \quad (3)$$

$$245 \quad CSI = \frac{1}{n} \sum_{i=1}^n \frac{PP_i}{PP_i + PN_i + NP_i} \quad (4)$$

246 The above equations take values from a rain/no-rain contingency table relating modelled and
 247 observed precipitation. *PP* counts simulated precipitation/observed precipitation (hits) *PN*
 248 simulated precipitation/observed no precipitation (false alarms), *NP* simulated no
 249 precipitation /observed precipitation (misses) and *NN* simulated no precipitation / observed
 250 no precipitation (correct negatives). When comparing the spatial performance of the
 251 simulations, the results of the WRF model were compared with rain-gauge observations at
 252 each time step *i*, and then the values of the categorical indices at all the time steps are
 253 averaged. In the case of temporal comparisons, the indices are calculated using simulated and
 254 observed time series data at each rain gauge *i*, then averaged to yield a single index value for
 255 all rain gauges.

256
 257 This study additionally employed the following continuous statistical indices: Nash–Sutcliffe
 258 model efficiency coefficient (NS), Correlation Coefficient (CORR), coefficient of
 259 determination (R^2), Slope (S), root mean square error (RMSE) and mean bias error (MBE)
 260 (see equations below).

261

$$NS = 1 - \frac{\sum_{i=1}^n [r_i(i) - p_i(i)]^2}{\sum_{i=1}^n [p_i(i) - \bar{p}_i]^2} \quad (5)$$

263

$$RMSE = \sqrt{\left(\frac{1}{n} \sum_{i=1}^n [r_i(i) - p_i(i)]^2 \right)} \quad (6)$$

265

$$CORR = \frac{n \sum_{i=1}^n [r_i(i) \cdot p_i(i)] - \sum_{i=1}^n [r_i(i)] \sum_{i=1}^n [p_i(i)]}{\sqrt{n \sum_{i=1}^n [p_i(i)]^2 - \left(\sum_{i=1}^n [p_i(i)] \right)^2} \cdot \sqrt{n \sum_{i=1}^n [r_i(i)]^2 - \left(\sum_{i=1}^n [r_i(i)] \right)^2}} \quad (7)$$

267

$$R^2 = \left(\frac{n \sum_{i=1}^n [r_i(i) \cdot p_i(i)] - \sum_{i=1}^n [r_i(i)] \sum_{i=1}^n [p_i(i)]}{\sqrt{n \sum_{i=1}^n [p_i(i)]^2 - \left(\sum_{i=1}^n [p_i(i)] \right)^2} \cdot \sqrt{n \sum_{i=1}^n [r_i(i)]^2 - \left(\sum_{i=1}^n [r_i(i)] \right)^2}} \right)^2 \quad (8)$$

269

$$S = \frac{n \sum_{i=1}^n [r_i(i) \cdot p_i(i)] - \sum_{i=1}^n [r_i(i)] \sum_{i=1}^n [p_i(i)]}{n \sum_{i=1}^n [p_i(i)]^2 - \left(\sum_{i=1}^n [p_i(i)] \right)^2} \quad (9)$$

$$MBE = \frac{\sum_{i=1}^n [r_i - p_i]}{n} \quad (10)$$

272

273

274

275

276

277

278

279

280

281

282

Where n is the number of observations; r_i = simulated precipitation, p_i = simulated precipitation variables from WRF under particular parameterization scheme and \bar{p}_i is mean observed precipitation. These indices can give an idea of spatial variation of WRF modelled results, comparing it with observed rainfall values from each weather station site. CORR value can give a measure of the strength and the direction of a linear relationship between observed and simulated precipitation time series. The coefficient of determination is useful as it gives a proportional measure of the variance of one variable that is predictable from another variable.

283 3. Results and Discussions

284 The performance of several CPSs and MPSs configurations of the WRF model was evaluated
285 for the 'York flood- 1999' event precipitation covering 0000 UTC 01st March 1999 to 0000
286 UTC 15th March 1999. The main aim was to select the best parameterization design for
287 operational weather prediction and climate downscaling over the region during exceptionally
288 high precipitation. Both frontal and convective storms are common in the study area; the
289 frontal storms normally produce precipitation over large areas, whereas convective storms
290 produce precipitation over smaller areas. The daily precipitation values during the study
291 period exhibited varying temporal trends, which are the stations, were spatially
292 heterogeneous. The temporal and spatial variation of daily precipitation is shown in the
293 Figure 4 as obtained by Krigging interpolation of daily values from 22 nearby stations in the
294 Upper Derwent catchment. In this figure it is evident that there is considerably high
295 precipitation on 4- 6th of March in the upper Derwent River catchment with value of 67.7 mm
296 at DANBY MOOR CENTRE (54.46, -0.89) on 6th of March 1999. Similar high values were
297 observed at KILDALE: EAST GREEN BECK (54.48 -1.04), SCALING RESR NO 3
298 (54.51 -0.84), RANDY MERE RESR (54.41 -0.75), IRTON P STA (54.24 -0.46) and
299 RAVENSWICK (54.28 -0.92) with values of 40.2 mm/day, 48.2 mm/day, 47.8 mm/day,
300 40.2 mm/day and 42.5 mm/day respectively. The stations with higher values are
301 predominantly in the northern part of the Derwent Basin. As explained earlier a four domain
302 configuration setups were used in this study with the inner domain dimension of 103 x 94
303 km² [1 km resolution, downscaling ratio of 1:3 and modelling time step 1 hr.]. The WRF
304 model with this set up downscaled the ERA-40 Reanalysis data for 14 days using different
305 CPSs and MPSs scenarios. Apart from the identification of a useful model setup for the
306 region, it is also important to evaluate variability in spatial and temporal distribution of these
307 downscaled precipitation outcomes from the WRF. This is because these values could
308 directly be applied to distributed hydrological models while WRF outcomes (areal average)
309 could be directly used in lumped, semi-distributed and distributed hydrological models for
310 flood forecasting and modelling. This section describes results of the sensitivity analyses of
311 various CPSs [Kain-Fritsch (KF2) Betts-Miller-Janjic (BMJ), Grell-Devenyi ensemble
312 (GD) and the old Kain-Fritsch (KF1)] and their spatial and temporal comparisons with 22
313 land based gauging stations. The corresponding temporal and spatial comparison results of
314 MPSs [Kessler, Lin et al, WRF Single-Moment 3-class (WSM3) and WRF Single-Moment
315 5-class (WSM5)] using various categorical and the continuous indices are given below.

316

317 **3.1 Spatial and Temporal Sensitivity of WRF to Cumulus Parameterization Schemes**
318 **(CPS) Selection**

319 The optimum cumulus parameterizations for precipitation are strongly dependent on the sub
320 region (Mooney et al., 2013) of the study domain. Many studies have demonstrated the need to
321 carefully select parameterization combinations when attempting to use WRF as a regional
322 climate model especially when linked to regional hydrological models. In this study we have
323 used WRF outputs from the 3rd domain for comparison with land based precipitation values.
324 This is because in many studies it is assumed that the convective rainfall generation is
325 explicitly resolved in the inner domain without cumulus parameterisation (Liu et al., 2012).
326 The sensitivity analysis and variations in WRF simulation of the rainfall distribution in space
327 and time are detailed in the Tables 5 and 6. The categorical indices (POD, FBI, FAR and
328 CSI) together with the continuous indices (NS, R², R, RMSE, MBE and S) that are calculated
329 for a 1 hour duration in both spatial and temporal dimensions are shown in these two tables.
330 Statistically one can say that the best WRF model gives higher values of POD, CSI NS, and
331 R² and lower values of FBI, FAR and continuous indices like RMSE and MBE. Table 5
332 shows the spatial variation of WRF simulations corresponding to the different CPS selections
333 in the form of continuous indices [NS, R², R, RMSE, MBE and S (these are averaged values
334 for the simulated 14 days period)] in comparison to the selected 22 weather stations.
335 Whereas, Table 6 shows the temporal variations of WRF simulations corresponding to
336 different CPS selection in the form of above mentioned continuous indices (spatially
337 averaged). We have used several indices for this sensitivity analysis considering the chaotic
338 nature of the convective environment. The chaotic nature of the atmosphere suggests that
339 analyses of only one type of error (e.g. biases) are not sufficient to rate model forecasts and
340 thus sensitivity analysis of different parameterizations, since errors in one variable may
341 propagate to others and quickly degrade forecasts.

342

343 **3.1.1 Spatial Comparison:**

344 In this study we adopt a sensitivity analysis using the categorical indices for first instance and
345 a second level verification employing continuous indices. The categorical indices can give a
346 measure of the correctness of the model's precipitation occurrence or non-occurrence, but are
347 less reliable when considering the quantity of precipitation thus not decisive in comparison to
348 continuous indices in identifying the best CPSs/ MPSs. POD assesses what fraction of the
349 actual rainfall events were detected by the model, and FAR gives the fraction of 'false
350 alarms' in rainfall occurrences. Thus, in order to quantify the differences between

351 precipitation produced by simulations with different CPSs the different categorical spatial
352 statistics are calculated for the ‘York Flood – 1999’ period and are shown in Figure 5 along
353 with corresponding values associated with changes of MPSs. The evaluations of these
354 statistical indices provide information about the model’s effectiveness in simulating a range
355 of precipitation events. The catchment area average values of probability of detection (POD)
356 and false alarm rate (FAR) are the major categorical indices, which range from 0.64–0.76 and
357 0.27–0.32, respectively. The highest values are associated with KF2 (POD= 0.69, FAR=
358 0.27) and the lowest are associated with GD (POD= 0.64, FAR= 0.29). An FBI values less
359 than one implies under estimation in all four CPSs based simulations. From figure 5 one can
360 note that, after spatial comparison of four CPSs based simulation results, the higher values of
361 precipitation underestimation occurred for GD based simulations with lower values for BMJ
362 based simulations. The higher CSI value is associated with KF1 based simulation but the
363 numerical value of CSI of BMJ based simulation is very close with value of 0.65. Although it
364 is difficult to reach a conclusion on the performance of different CPSs from the Figure 5, the
365 lower average value of FAR and higher FBI, CSI and POD scores indicate better model
366 performance for heavier precipitation events with the KF2 and BMJ cumulus schemes.

367

368 Table 5 summarizes the effect of different cumulus parameterizations on spatial estimates of
369 precipitation. Considering the spatial variation of continuous indices for KF1-based
370 simulations, it can be seen that overall poor performance of the model is associated with
371 weather station IDs 19 and 20 (i.e. KELD HEAD and KIRBY MISPERTON) with low values
372 of NS efficiency, R^2 , R and negative values of Slope. These trends were similar in
373 simulations with the other three CPSs (KF2, BMJ and GD). The weather station locations
374 associated with poor performance are towards the middle of the River Derwent catchment. It
375 is interesting to note that only these two stations have shown negative or near zero slope
376 values in all four CPSs simulations with spatial comparison. This study also focused on
377 continuous statistical indices (e.g. RMSE, NS) that include both systematic and non-
378 systematic errors. This measure of total error might be more relevant to evaluating model
379 performance and its ability to simulate atmospheric physics. An index like NS can give an
380 assessment of the predictive power and efficiency of the WRF model as long as there is
381 observed data to compare with the modelled results. If an NS value is less than zero, then the
382 observed mean is a better predictor than the model. The NS value ranges between $-\infty$ to 1
383 and if model efficiency is close to 1, model reliability and accuracy will be close to the
384 maximum. Out of 22 stations higher modelling efficiencies were associated with stations

385 such as KILDALE: EAST GREEN BECK (ID = 4) and WHITBY COASTGUARD
386 (ID=11) during KF1 and KF2 simulations. Both in BMJ and GD based simulations,
387 KILDALE station exhibited higher efficiencies with values of 0.42 and 0.35 respectively.
388 This station is one of those situated north of Derwent catchment which experienced high
389 precipitation rates during the York Flood 1999 period. The bias and RMSE values didn't
390 show any fixed pattern within the study area. Over the south east corner of the catchment
391 ($54^{\circ}0'0''$ N - $54^{\circ}10'0''$ N to $0^{\circ}30'00''$ W - $0^{\circ}40'00''$ W), there is a strong positive bias in
392 predicted WRF precipitation at all times of day and integration times. For a detailed
393 comparison, the rainfall simulated by WRF with different CPSs is shown in Figure 6 for
394 selected weather stations (along with different MPSs selection). Figure 6 shows daily
395 averaged values of modelled precipitation during 1st -14th March 1999. One can clearly note
396 from the Table 5, Table 6 and Figure 5 (a-d) that there is clear underestimation and
397 overestimation within the basin corresponding to different weather station positions. Though
398 there is overestimation in certain stations during certain time steps, the average value of MBE
399 is always negative in all CPSs suggesting a high tendency towards underestimation. A
400 comparison with a spatial average of the WRF precipitation output with that of observed
401 output shows that BMJ scheme is superior to the other three when we consider indices like
402 NS, R^2 , R and Slope with values of -0.41, 0.38, 0.19 and 0.49 respectively. The Bias values
403 were smaller in the case of the KF1 scheme with a value of -0.77 mm/day, which is closer to
404 that of BMJ scheme. Though a bit higher, RMSE values of the BMJ scheme were closer to
405 that KF2 scheme during spatial evaluation. In general one can say that the schemes have
406 followed a performance trend of BMJ > KF1 > GD > KF2 during CPSs simulations. During
407 these four simulations, the microphysics was fixed as WRF Single-Moment 5-class scheme.
408 One can note from Figure 6 that BMJ modelled precipitation is largest in the majority of the
409 weather stations, but KF1 over performed the BMJ cumulus scheme in stations like IRTON P
410 STA, HOVINGHAM HALL, KELD HEAD and KIRBY MISPERTON when we considered
411 daily average modelled precipitation during 'York Flood- 1999' period.

412

413 **3.1.2 Temporal Comparison:**

414 Figure 7 presents the temporal average skill scores for the 14 days studied during the 'York
415 Flood -1999' based on different CPS simulations. The temporal spread of the CPS based
416 predictions by WRF has been evaluated through statistical verification against the available
417 land based observation datasets. The temporal average categorical indices have shown that all
418 CPS members do well in terms of POD and FAR particularly during 4th -6th March 1999, but

419 the scores of POD drop off rapidly towards the end of the simulation dates and false alarm
420 ratios increased during those days. The numerical values of CSI are lower than those of
421 spatial indices [the lower value is associated with GD value of 0.34]. The bias index has a
422 similar tendency to that of the spatial comparisons but with a better value of 0.85 for the KF2
423 scheme. In the case of KF2 and BMJ the probability of detection values are almost same but
424 the false alarm index is less in the case of KF2 scheme than the BMJ one. Considering all
425 four categorical indices, one can say that the performance of cumulus schemes follow this
426 pattern, $KF2 > BMJ > KF1 > GD$.

427 The NS values are negative for all four simulations which indicate that, this criterion is very
428 sensitive to the quantification of systematic under-prediction errors. The simulated
429 precipitation values from the model that included different CPSs schemes inadequately
430 captured the measured rainfall responses in terms of low RMSE, high bias, lower regression
431 coefficient and Nash efficiency index. The lower (better) MBE and NS indices were
432 associated with the KF1 scheme. The continuous statistical values have shown better
433 performance on 4th of March and poorer performance on 6th of March with high values of
434 MBE and RMSE. It can be seen from the time averaged continuous statistical indices
435 (excluding MBE), that the results of WRF model with KF2 are superior to that of other WRF
436 models with CPSs. Although, it is difficult to reach a conclusion, it appears that the KF2
437 scheme performed better than the BMJ scheme (which was better during spatial comparison
438 of CPSs) when making temporal comparisons. Apart from these statistical analyses,
439 variations in cumulative precipitation during 1st -14th March 1999 as predicted by different
440 CPSs in the study region were plotted and are given in Figure 8. This shows the higher
441 capability of the BMJ and lower performance of GD schemes in this case study.

442

443 **3.2 Spatial and Temporal Sensitivity of WRF to Microphysics parameterization** 444 **schemes (MPS) Selection**

445 State-of-art microphysical parameterization schemes are commonly used to predict
446 precipitation distribution within convective systems and many studies have shown that these
447 can make a considerable difference in the resultant simulation (Luo et al. 2010; Cohen and
448 McCaul 2006). Thus, to assess impact of the parameterization of microphysical processes on
449 the development of convective systems in Northern Yorkshire region during first two weeks
450 of March -1999, we have performed simulations using four microphysics parameterizations
451 with varying complexity as explained in previous sections. These simulation results were
452 comprehensively compared in both spatial and temporal scales using traditional categorical

453 verification statistics and continuous statistics to check the accuracy of precipitation
454 forecasts. Four simulations of four MPSs were performed with identical configurations,
455 except for differences in the cloud microphysics parameterizations. The BMJ scheme was
456 used as it has proved to be the best cumulus scheme.

457

458 **3.2.1 Spatial Comparison:**

459 Figure 5 shows the spatial average categorical verification results for FBI, FAR, POD, and
460 CSI in MPSs for the Upper River Derwent highlighted for the period 1st March -14th March.
461 The categorical results in Figure 5 show that the changes in MPSs which are used to initialize
462 the WRF model do not greatly affect the numerical values and fluctuating nature of the CSI.
463 The highest CSI value was associated with WSM5 (0.62) and lowest with WSM3 (0.43). It is
464 interesting to note that the categorical bias index value increased to 0.88 showing least bias
465 for the WSM5 scheme based simulation in comparison to all other simulation scenarios. Over
466 BIRDSALL HOUSE and HIGH MOWTHORPE station regions, both Kessler and the Lin et
467 al scheme detect almost the same frequency of rain events during low rainfall periods and the
468 bias index was above 0.95 showing low bias during that period. In the case of all four MPSs,
469 both FBI and CSI have a similar trend to that of POD with slight disparity in the case of FAR.
470 The combination of WSM5 and BMJ gave highest value of both POD and FBI; together with
471 the lowest value of FAR. In the south east and north west corners of the basin (in positions
472 like BIRDSALL HOUSE, HIGH MOWTHORPE, MONK END FARM, and KILDALE:
473 EAST GREEN BECK) there are lower FAR scores in the case of all four MPSs scenarios.
474 These results suggest that the best MPS selections based on categorical thresholds are WSM5
475 > Lin et. al. > WSM3 > Kessler for this study region.

476

477 The NS index, Correlation Coefficient, Coefficient of Regression and slope values all
478 increased in the combination of BMJ scheme with WSM5, Lin.et al and WSM3 micro
479 physics schemes. The best WRF model setting for a given strategy was selected in such a
480 way that its performance is satisfactory with the selection of given CPSs and MPSs. This
481 resulted in the spatial average of RMSE being reduced to 6.40 mm, 4.54 mm and 5.34 mm
482 for MPS sections of Lin et al., WSM3 and WSM5 respectively. These values are an
483 improvement of -30.20%, -50.49%, -41.76% over the combination with Kessler
484 microphysics with KF1 cumulus scheme (Note: Kessler micro physics scheme was fixed
485 when we e made comparative simulations for different CPSs in the earlier section). The MBE
486 values have decreased by 28.78 %, 39.79 % and 51.98 % for the Lin et al; WSM3 and WSM5

487 micro physics schemes respectively. Considering both types of index the best model
488 configuration for our study basin occurs when the WSM5 is combined with BMJ cumulus
489 scheme. However, the performance of WSM3 combined with BMJ gives a similar value.

490

491

492 **3.2.2 Temporal Comparison:**

493 When categorical indices for whole simulation period are compared (Figure 7), POD results
494 in both WSM5 and WSM3 microphysics are better but the highest value of the critical
495 success index was associated with the Kessler scheme followed by WSM5 and WSM3. There
496 was little difference in the bias index; however the WSM3 combination with BMJ was
497 slightly better. The critical success index (CSI) is more stable and differs by only 2%-3%
498 from the previous highest values. Statistical indicators show reasonably acceptable values for
499 POD (0.69), FBI (0.88) and FAR (0.31), with a corresponding CSI value of 0.49, indicating a
500 high level of success for the WSM3 in detecting rare events in this region. The corresponding
501 values associated with WSM3 are 0.69, 0.88, 0.31 and 0.49, suggesting a comparable
502 performance. The higher values of POD than that of FAR show the potential for WRF
503 models to model convective precipitation in better way. However, in the case of the
504 temporal comparison of Lin et. al. Scheme, the FAR value was shown to be slightly higher
505 than POD.

506

507 In comparison to temporal values for CPSs schemes, better NS and MBE have been
508 identified in both WSM3 and WSM5 micro physics schemes; but lower ones in Lin. et. al.
509 scheme with NS values of -0.25, -0.25 and -1.85 respectively. On the other hand, the
510 coefficient of regression and correlation coefficient values increased only in the case of the
511 WSM3 scheme. So considering both categorical and continuous indices it is possible to say
512 the better microphysics is found in WSM3 followed by WSM5 when used in conjunction
513 with the BMJ cumulus scheme. The cumulative variation of precipitation simulated using
514 different microphysics schemes are shown in the Figure 9 which shows clearly the better
515 performance of WSM3 in conjunction with BMJ cumulus scheme. To get a better idea of the
516 variation of the WRF simulated precipitation (WSM3 in conjunction with BMJ) during the
517 simulation time period, total precipitations at various time scales are shown in the form of 2D
518 maps in Figure 10.

519

520 *In this study convective and stratiform precipitation with the BMJ scheme is in more*
521 *agreement with the land based observations in comparison to the other Cumulus schemes*
522 *during the simulation scheme. Similar convective parameterization schemes are identified in*
523 *a recent WRF sensitivity analysis to downscale summer rainfall over South Africa (Ratna et*
524 *al., 2014). The lowest track error of cyclones simulated in a recent study by Chandrasekar*
525 *and Balaji (2012) with numerical experiments for different cumulus schemes were associated*
526 *with the experiment with the BMJ scheme for a 24-hr forecast time. WSM3 usually generates*
527 *the shallowest storm and slowest deepening rate (Li and Pu, 2008). The differences in*
528 *performance of WSM3 and WSM4 depend on the inclusion and exclusion of mixed-phase*
529 *microphysical processes and the method of representing melting-freezing processes. Li and*
530 *Pu (2008) showed that WSM3 could predict type 1 hurricanes whereas the WSM5 produced*
531 *a storm value 12 hPa deeper than that in WSM3. Evans et al (2012) suggests WSM3 is a*
532 *simpler but robust scheme than other more complex schemes that include other classes*
533 *(cloud water, cloud ice, rain, snow, vapour). The analysis of Evans et al (2012) of the overall*
534 *bias reveals that the precipitation is sensitive to BMJ generally producing lower bias in*
535 *comparison to other cumulus scheme. A recent study by Alam (2014) has shown better*
536 *performance of WSM3 in heavy rainfall generation over Bangladesh. The study showed that*
537 *the WSM3 and Kessler schemes coupling with KF1 and BMJ schemes simulated significant*
538 *amounts of rain water mixing ratio between 500 and 100 hPa, but WSM3 simulated a much*
539 *higher rain water mixing ratio than that of the Kessler scheme. But in general Lin–KF1*
540 *combination gave better performance in this region. It indicates that the performance of*
541 *BMJ or WSM3 schemes based on scores cannot be generalised in the study region, and it*
542 *varies with the event’s physical processes.*

543

544 **4. Conclusions:**

545 This study investigated the sensitivity of the WRF mesoscale numeric weather model to the
546 selection of CPS and MPS to model the Yorkshire – Humberside region (Upper River
547 Derwent) during the ‘York flood -1999’ event. This analysis of convection permitting
548 simulations was aimed at increasing the understanding of the role of parameterized cloud
549 microphysics and cumulus schemes in the simulation of rare events in Northern Yorkshire
550 focusing on the land based data from the Upper Derwent catchment. The results were
551 compared with land based precipitation data from 22 rain gauges scattered around region.

552 This analysis demonstrates that the WRF simulation is very sensitive to the parameterization
553 of cumulus and microphysical processes. The study has clearly indicated that all CPSs and
554 MPSs schemes underestimated in describing the average quantity of daily precipitation
555 during the ‘York Flood – 1999’ in all experiments, though there were few overestimations at
556 certain locations for specific time steps. While statistical analysis using categorical and
557 continuous indices gave slightly different results, we selected the best model setup by
558 considering the superior categorical temporal indices, high values of R, R^2 , RMSE and lower
559 values of MBE. In general, the BMJ scheme successfully simulated the spatial and temporal
560 features of the York flood-1999 although it produced underestimations in both spatial and
561 temporal scales. The GD cumulus schemes performed poorly with persistent location bias,
562 and failed to simulate the relevant features in both temporal and spatial scales. The
563 performance of KF2 and KF1 was comparable but both schemes gave results with higher
564 values of negative bias. The spatial comparison results were surprising as the relatively
565 simple KF1 value outperformed the more complex KF2 and GD schemes which would
566 normally be expected to produce superior results.

567

568 Relatively poor verification results suggest that it is also important to consider the
569 interactions between various model physical parameterizations in order to find better overall
570 combinations. For this reason, the study tested different microphysics configuration, fixing
571 the cumulus scheme to BMJ. As for the BMJ convective schemes in the earlier case, better
572 values of continuous indices were observed in the case of the WSM3 microphysics scheme
573 which has outperformed all other three microphysics schemes in both spatial and temporal
574 scales. There was slight disparity in the case of values obtained from categorical indices.
575 WSM5 had more favourable categorical index values than WSM3 during temporal
576 comparison, whereas in the spatial comparison, the WSM3 has outperformed WSM5. Unlike
577 all other combinations tested in the Derwent basin during the ‘York Flood – 1999’ period, the
578 model setup employing a combination of WSM5 and BMJ schemes produced superior results
579 over all the other seven model set-ups. This study has highlighted the influence of explicit
580 moisture schemes and microphysics on rainfall intensity prediction using WRF.

581

582 Properly parameterized mesoscale numerical model outputs can provide inputs for spatially
583 explicit distributed hydrologic models that use grid cells as a primary hydrologic unit. For
584 example, integrated systems like WRF-Hydro can be successfully applied to any region
585 considering atmospheric, land surface and hydrological processes on grid scale (Gochis et al.,

2014). A study by Nicholas et al (2013) highlighted the use of mesoscale model meteorological data in stream flow and snowpack response modelling in significantly data limited mountainous region. WRF could also be integrated with urban modelling systems to tackle related issues and to bridge the gaps between mesoscale and microscale modelling (Chen et al., 2011). Fowler (2005) noted that Yorkshire floods are a product of complex interaction of the spatial-temporal rainfall pattern and hydrological connectivity of ungauged catchments. This study has presented a case study at a catchment scale focusing on flood events that occurred in a certain year. As it looked at a single event in detail the results may not be generalizable to all forms of convection occurring in Yorkshire-Humberside region. The primary contribution of this study is to provide some insight into how critical is the choice of cumulus and microphysics parameterization in regional scale. However it has highlighted how choice of parameterization can influence model results and has indicated how this can be very important in predicting high intensity rainfall events. Accurate prediction depends on horizontal/vertical resolutions, coupling with ocean, data assimilation, model initialization etc. The choice of the downscaling ratios also would have an influence of downscaled precipitation.

602

603 **5. Acknowledgements**

604 This study was funded by Yorkshire Forward within the research project ‘Low Carbon and
605 Climate Resilient Regional Economy’ which has the objective of assessing the impacts of
606 climate change on resources that influence the future regional economy of the Yorkshire –
607 Humberside region in North-East England.

608

609 **6. References**

610 Alam MM (2014) Impact of cloud microphysics and cumulus parameterization on simulation
611 of heavy rainfall event during 7–9 October 2007 over Bangladesh. *J. Earth Syst. Sci.* 123, 2:
612 259–279

613 Bugaets A, Gonchukov L (2014) Application of WRF - SWAT OpenMI 2.0 based models
614 integration for real time hydrological modelling and forecasting. *Geophysical Research*
615 *Abstracts*. 16, EGU2014-4712

616 Chandrasekar R, Balaji C (2012). Sensitivity of tropical cyclone Jal simulations to physics
617 parameterizations. *J. Earth Syst. Sci.* 121, 4: 923–946

618 Chen F, Kusaka H, Bornstein R, Ching J, Grimmond CSB, Grossman-Clarke S, Loridan T,
619 Manning KW, Martilli A, Miao S, Sailor D, Salamanca FP, Taha H, Tewari M, Wang X,
620 Wyszogrodzki AA, Zhang C (2011). The integrated WRF/urban modelling system:

621 Development, evaluation, and applications to urban environmental problems. *Int. J. Climatol.*
622 31: 273–288. DOI: 10.1002/joc.2158.

623 Cohen C, McCaul Jr EW (2006) The sensitivity of simulated convective storms to variations
624 in prescribed single-moment microphysics parameters that describe particle distributions,
625 sizes, and numbers. *Mon. Wea. Rev.* 134: 2547-2565.

626 Dudhia J (1989) Numerical study of convection observed during the winter monsoon
627 experiment using a mesoscale two-dimensional model. *Journal of the Atmospheric Sciences*
628 46(20): 3077–3107.

629 Environment Agency (2007) Managing Flood risk. Yorkshire Derwent Catchment Flood
630 Management Plan May 2007. [www.knowledge-](http://www.knowledge-controversies.ouce.ox.ac.uk/Ryedale2/.../DCFMP.pdf)
631 [controversies.ouce.ox.ac.uk/Ryedale2/.../DCFMP.pdf](http://www.knowledge-controversies.ouce.ox.ac.uk/Ryedale2/.../DCFMP.pdf) (downloaded on 29/05/2013).

632 Evans JP, Ekstrom, M, Ji F. (2012). Evaluating the performance of a WRF physics ensemble
633 over South-East Australia. *Clim Dyn* 39:1241–1258 DOI 10.1007/s00382-011-1244-5

634 Fovell RG, Su H (2007) Impact of cloud microphysics on hurricane track forecasts. *Geophys.*
635 *Res. Lett.* 34, L24810.

636 Fowler MA, Roebber PJ (2003) Short-range (0-48 h) numerical prediction of convective
637 occurrence, mode, and location. *Weather and Forecasting* 18: 782–794.

638 Fritsch JM, Carbone RE (2004) Improving quantitative precipitation forecasts in the warm
639 season: a USWRP research and development strategy. *Bulletin of the American*
640 *Meteorological Society* 85(7): 955–965.

641

642 Giorgi F, Bates GT, Nieman SJ. 1993. The multiyear surface climatology of a regional
643 atmospheric model over the western United States. *Journal of Climate* 6: 75–95.

644 Givati A, Barry L, Yubao L, Alon R, (2012) Using the WRF Model in an Operational
645 Streamflow Forecast System for the Jordan River. *J. Appl. Meteor. Climatol*, 51, 285–299
646 doi: <http://dx.doi.org/10.1175/JAMC-D-11-082.1>

647 Grell GA (1993) Prognostic evaluation of assumption used by cumulus parameterizations.
648 *Mon. Wea. Rev.* 121: 764-787.

649 Grell GA, Devenyi D (2002) A generalized approach to parameterizing convection
650 combining ensemble and data assimilation techniques. *Geophys. Res. Lett.* 29(14), 1-4. doi:
651 10.1029/2002GL015311.

652 Gochis D, Rasmussen R, Yu W, Ikeda, K (2014). Modeling changes in extreme snowfall
653 events in the Central Rocky Mountains Region with the Fully-Coupled WRF-Hydro
654 Modeling System. *Geophysical Research Abstracts* 16. EGU2014-16094

655 Hong SY, Dudhia J, Chen SH (2004) A Revised Approach to Ice Microphysical Processes for
656 the Bulk Parameterization of Clouds and Precipitation. *Mon. Wea. Rev.* 132: 103–120.

657 Hong SY, Noh Y, Dudhia J (2006) A new vertical diffusion package with an explicit
658 treatment of entrainment processes. *Monthly Weather Review* 134: 2318–2341.

659 Hu M, Nielsen-Gammon JW, Zhang F (2010) Evaluation of three planetary boundary layer
660 schemes in the WRF model. *J. Appl. Meteor. Climatol.* 49: 1831–1844.

661 Ishak A, Bray M, Remesan R, Han D (2012) Seasonal Evaluation of Rainfall Estimation by
662 four Cumulus Parameterization Schemes and their Sensitivity Analysis. *Hydrological*
663 *Processes.* 26: 1062 – 1078. DOI: 10.1002/hyp.8194.

664 Janjic ZI (1994) The step-mountain eta coordinate model: Further developments of the
665 convection, viscous sublayer and turbulence closure schemes. *Mon. Weather Rev.* 122: 927–
666 945.

667 Janjic ZI (2000). Comments on “Development and evaluation of a convection scheme for use
668 in climate models”. *J. Atmos. Sci.* 57, 3686.

669 Jolliffe IT, Stephenson DB (2003) *Forecast Verification: A Practitioner’s Guide in*
670 *Atmospheric Science.* John Wiley and Sons: Chichester, UK; 240.

671 Kain JS (2004) The Kain–Fritsch convective parameterization: An update. *J. Appl. Meteor.*
672 43: 170–181.

673 Kain JS, Fritsch JM (1990) A one-dimensional entraining/detraining plume model and its
674 application in convective parameterization. *J. Atmos. Sci.* 47(23): 2784–2802.

675 Kerkhoven E, Gan TY, Shiiba M, Reuter G, Tanaka K (2006) A comparison of cumulus
676 parameterization schemes in a numerical weather prediction model for a monsoon rainfall
677 event. *Hydrol. Processes.* 20: 1961–1978.

678 Kessler E (1969) On the distribution and continuity of water substance in atmospheric
679 circulation. *Meteor. Monogr. No. 32, Amer. Meteor. Soc.,* 84.

680 Kite GW, Haberlandt U (1999) Atmospheric model data for macroscale hydrology. *Journal of*
681 *Hydrology* 217: 303–313. doi:10.1016/S0022-1694(98)00230-3.

682 Krishnamurti TN, Kishtawal CM, LaRow TE, Bachiochi DR, Zhang Z, and coauthors (1999)
683 Improved weather and seasonal climate forecasts from multi-model superensemble. *Science*
684 285: 1548–1550.

685 Kuo HL (1974) Further studies of the parameterizations of the influence of
686 cumulus convection on large scale flow. *J. Atmos. Sci.* 31: 1232-1240

687 Li X, Pu, Z (2008). Sensitivity of Numerical Simulation of Early Rapid Intensification of
688 Hurricane Emily (2005) to Cloud Microphysical and Planetary Boundary Layer
689 Parameterizations. *Monthly Weather Review* 136. DOI: 10.1175/2008MWR2366.1

690 Lin YL, Farley RD, Orville HD (1983) Bulk parameterization of the snow field in a cloud
691 model. *J. Climate App. Meteor.* 22: 1065-1092.

692 Liong SY, Raghavan SV, Vu MT (2013). Climate Change and Its Impacts on Streamflow:
693 WRF and SCE-Optimized SWAT Models. Data Assimilation for Atmospheric, Oceanic and
694 Hydrologic Applications (Vol. II). 411-428

695 Liu J, Bray M, Han D (2012) Sensitivity of the Weather Research and Forecasting (WRF)
696 model to downscaling ratios and storm types in rainfall simulation. *Hydrol. Process.* 26:
697 3012–3031

698 Luo Y, Wang Y, Wang H, Zheng Y, Morrison H (2010) Modelling convective- stratiform
699 precipitation processes on a Mei-Yu front with the Weather Research and Forecasting model:
700 Comparison with observations and sensitivity to cloud microphysics parameterizations. *J.*
701 *Geophys. Res.* 115: D18117.

702 Mooney PA, Mulligan FJ, Fealy R (2013) Evaluation of the Sensitivity of the Weather
703 Research and Forecasting Model to Parameterization Schemes for Regional Climates of
704 Europe over the Period 1990–95. *J. Climate* 26: 1002–1017. doi:
705 <http://dx.doi.org/10.1175/JCLI-D-11-00676.1>.

706 Nicholas EW, Alan FH, Mimi H, Shara IF, Jessica DL (2013). Intercomparison of
707 Meteorological Forcing Data from Empirical and Mesoscale Model Sources in the North
708 Fork American River Basin in Northern Sierra Nevada, California. *J. Hydrometeor.* 14: 677–
709 699. doi: <http://dx.doi.org/10.1175/JHM-D-12-0102.1>

710 Pall JS, Eltahir EAB (2001) Pathways relating soil moisture conditions to future summer
711 rainfall within a model of the land-atmosphere system. *J. Climate* 14: 1227–1242.

712 Ratna SB, Ratnam JV, Behera SK, Rautenbach CJD, Ndarana T, Takahashi K, Yamagata T.
713 (2014). Performance assessment of three convective parameterization schemes in WRF for
714 downscaling summer rainfall over South Africa. *Climate Dynamics* 42,11-12: 2931-
715 2953. doi: [10.1007/s00382-013-1918-2](https://doi.org/10.1007/s00382-013-1918-2)

716 Remesan R, Bellerby T, Frostick L (2013) Hydrological modelling using data from monthly
717 GCMs in a regional catchment. *Hydrol. Process.* DOI: 10.1002/hyp.9872

718 Ruiz JJ, Saulo C (2010) WRF Model Sensitivity to Choice of Parameterization over South
719 America: Validation against Surface Variables. *Monthly Weather Review* 138: 3342-3355.

720 Ryedale Natural History Society (RNHS) (2013) The March Floods.
721 <http://www.ryenats.org.uk/flood99.htm> (downloaded on 23/05/2013).

722 Salimun E, Tangang F, Juneng L (2010) Simulation of heavy precipitation episode over
723 eastern Peninsular Malaysia using MM5: Sensitivity to cumulus parameterization schemes.
724 *Meteorol. Atmos. Phys.* 107: 33–49.

725 Seuffert G, Gross P, Simmer C, Wood EF (2002) The Influence of Hydrologic Modeling on
726 the Predicted Local Weather: Two-Way Coupling of a Mesoscale Weather Prediction Model
727 and a Land Surface Hydrologic Model. *J. Hydrometeor* 3, 505–523. doi:
728 [http://dx.doi.org/10.1175/1525-7541\(2002\)003<0505:TIOHMO>2.0.CO;2](http://dx.doi.org/10.1175/1525-7541(2002)003<0505:TIOHMO>2.0.CO;2)

729 Skamarock WC, Klemp JB, Dudhia J, Gill DO, Barker DM, Wang W, Powers JG (2005) A
730 description of the Advanced Research WRF Version 2. NCAR Tech. Note/TN-468+STR, 88
731 pp.

732 Stanski HR, Wilson LJ, Burrows WR (1989) Survey of common verification methods in
733 meteorology. World Weather Watch Technical Report No. 8, WMO/TD No.358, WMO,
734 Geneva, 114.

735 Tang C, Dennis RL (2014) How reliable is the offline linkage of Weather Research &
736 Forecasting Model (WRF) and Variable Infiltration Capacity (VIC) model?. Global and
737 Planetary Change 116, 1–9.

738 Wenhua G, Chung-Hsiung S (2013) A Modeling Analysis of Rainfall and Water Cycle by
739 the Cloud-resolving WRF Model over the Western North Pacific. Advances in
740 Atmospheric Sciences. 30 (6) 1695–1711.

741 Wilks DS (2006) Statistical Methods in Atmospheric Science, 2nd Edn. Academic Press:
742 Burlington, MA, 627.

743 Wood AW, Leung LR, Sridhar V, Lettenmaier DP (2004). Hydrologic implications of
744 dynamical and statistical approaches to downscaling climate model outputs. Climatic Change
745 62: 189–216

746 WRF (2013) WRF model users page. <http://www.mmm.ucar.edu/wrf/users/>.

747 Zhang DL, Zheng WZ, Xue YK (2003) A numerical study of early summer regional climate
748 and weather over LSA-East. Part I: model implementation and verification. Monthly Weather
749 Review 131: 1895–1909.

750

751

752

Table Titles

753

754 Table 1: Details of different stations in Yorkshire –Humber region used for comparison of
755 WRF results

756 Table 2: A brief summary WRF model configuration in Yorkshire-Humberside

757 Table 3: Details of nested domains, grid spacing and downscaling ratio used in Yorkshire-
758 Humberside WRF modelling

759 Table 4: Comparison of the four WRF cumulus parameterization schemes used in this study

760 Table 5: Spatial comparison (in terms of different continuous statistical indices) of different CPSs
761 based WRF results with corresponding weather stations

762 Table 6: Temporal comparison (in terms of different continuous statistical indices) of different CPSs
763 based WRF results with corresponding weather stations

764

Figure Titles

765 Figure 1 Dimensions of the nested domains for different model settings which are centred over the
766 River Derwent catchment, Yorkshire-Humberside. d01, d02, d03 and d04 refer to the four domains
767 (NB: refer table 4 for details)

768 Figure 2: The observed rainfall during 1st March- 14th March 1999 from different stations at Derwent,
769 Yorkshire [N.B. refer table 2 and figure 4 to for the locations of stations]

770 Figure 3: The accumulated rainfall during 1st March- 14th March 1999 from different stations at
771 Derwent, Yorkshire [N.B. refer table 2 and figure 4 to for the locations of stations]

772 Figure 4: The spatial and temporal variation of precipitation during ‘York Flood – 1999’ period [N.B:
773 the numbers are corresponding weather stations as mentioned in the table 2]

774 Figure 5: Spatial variation of categorical indices with selection of different CPSs and MPSs during
775 York Flood – 1999

776 Figure 6: Scatter plots of the WRF simulated precipitation under different CPSs /MPSs and observed
777 catchment precipitations during ‘York Flood -1999’ corresponding to different weather stations [N.B:
778 1:1 lines added to all figures]

779 Figure 7: Temporal variation of categorical indices with selection of different CPSs and MPSs during
780 York Flood- 1999

781 Figure 8: Cumulative variation of WRF predicted precipitation during ‘York Flood – 1999’ using
782 different CPSs

783 Figure 9: Cumulative variation of WRF predicted precipitation during ‘York Flood – 1999’ using
784 different MPSs

785 Figure 10: The accumulated precipitation results obtained from WRF with WRF SM3 and BMJ
786 schemes from 1st March to 14th march 1999

787

788

789

791 **Table 1: Details of different stations in Yorkshire –Humber region used for comparison**
 792 **of WRF results**

Number	Site	LAT	LONG
1	BIRDSALL HOUSE	54.076	-0.748
2	HIGH MOWTHORPE	54.105	-0.641
3	MONK END FARM	54.480	-0.963
4	KILDALE: EAST GREEN BECK	54.480	-1.043
5	CRATHORNE HOUSE	54.464	-1.322
6	SCALING RESR NO 3	54.505	-0.845
7	MULGRAVE CASTLE	54.501	-0.694
8	DANBY MOOR CENTRE)	54.466	-0.895
9	RANDY MERE RESR	54.409	-0.752
10	WHITBY	54.481	-0.624
11	WHITBY COASTGUARD	54.490	-0.604
12	SCARBOROUGH	54.273	-0.421
13	HIGH MOWTHORPE	54.105	-0.641
14	COXWOLD STORES	54.187	-1.182
15	IRTON P STA	54.242	-0.458
16	GANTON: GOLF CLUB	54.190	-0.494
17	RAVENSWICK	54.277	-0.916
18	HOVINGHAM HALL	54.173	-0.980
19	KELD HEAD	54.245	-0.806
20	KIRBY MISPERTON	54.198	-0.790
21	BIRDSALL HOUSE	54.076	-0.749
22	ELVINGTON W WKS	53.927	-0.927

793 Source: British Atmospheric Data Centre (badc.nerc.ac.uk)

794
 795
 796
 797
 798
 799
 800
 801
 802
 803
 804
 805

Table 2: A brief summary WRF model configuration in Yorkshire-Humberside

Number	Features	Details
1	Nesting option	4 nests with 1 km inner and 27 km outer dimensions
2	Vertical coordinate	Terrain following σ_p
3	Horizontal grid	Arakawa-C
4	Projection	Lambert
5	Time integration scheme	Third-order Runge–Kutta scheme
6	Microphysics	Kessler scheme, Lin et.al. Scheme, WSM3, WSM5,
7	Convection	GD, BMJ, KF1, KF2
8	Radiation	Dudhia shortwave radiation scheme (Dudhia, 1989) and the rapid radiative transfer model long-wave radiation scheme (Mlawer et al., 1997)
9	Planetary boundary layer (PBL)	Yonsei University planetary scheme

806

807

808

809

810

811 **Table 3: Details of nested domains, grid spacing and downscaling ratio used in**
 812 **Yorkshire-Humberside WRF modelling**

Domain	Time step (hour)	Grid (km)	Number of grids	Domain size (km²)	Downscaling ratio
Domain 1	3	27	34 x 28	918 x 756	-
Domain 2	1	9	55 x 58	495 x 522	1:3
Domain 3	1	3	82 x 85	246 x 255	1:3
Domain 4	1	1	103 x 94	103 x 94	1:3

813

814

815

816

817

818

819 **Table 4: Comparison of the four WRF cumulus parameterization schemes used in this**
 820 **study**

CPSs	Trigger function	Precipitation scheme	Closure assumption	Changes from predecessor and other details
KF1	CAPE-based Cloud depth >4km	CAPE is removed from grid in convective	1D mass conservative cloud model	Nil

		time scale		<p>No Shallow- convection</p> <p>No Momentum- tendencies</p> <p>Moisture tendencies: Qc Qr Qi Qs</p> <p>Cores: ARW</p>
KF2	CAPE-based Cloud depth >3km	- Do -	- Do -	<p>Cloud radius and cloud depth threshold for deep convection can vary</p> <p>The effects of shallow convection is also included</p> <p>No Momentum- tendencies</p> <p>Moisture tendencies: Qc Qr Qi Qs</p> <p>Cores: ARW</p>

				NMM
BMJ	Based on an instability Cloud depth >200 hPa Sufficient moisture above cloud base	An adjustment towards an equilibrium reference profile	Adjustment scheme No cloud model	Reference profile and relaxation time depends on parameters that characterize the environment Trigger function to account for higher resolution No Momentum-tendencies Cores: ARW NMM
GD	Trigger function varies for each member but are commonly based on: CAPE CAPE trend Moisture convergence	Multi-closure, can be based on: CAPE Moisture convergence Low-level vertical velocity	Cloud model with updraft and downdraft fluxes No lateral entrainment and detrainment Changes in moisture is averaged over	Combines the strength of different closure assumptions in one scheme No Shallow-convection No Momentum-tendencies

			all members	Moisture tendencies: Qc Qi Cores: ARW NMM
--	--	--	----------------	---

821

822

823

824

825

826

Table 5: Spatial comparison (in terms of different continuous statistical indices) of different CPSs based WRF results with corresponding weather stations

CPSs	Indices	Weather station number																					
		1	2	3	4	5	6	7	8	9	10	11	12	13	14	15	16	17	18	19	20	21	22
KF1	NS	0.11	-0.05	0.03	0.44	0.25	0.20	0.26	-0.30	0.16	0.29	0.19	-1.43	-0.05	-0.57	-2.32	-0.70	-2.53	-0.21	-2.55	-0.85	0.11	0.25
	R2	0.35	0.25	0.20	0.73	0.55	0.62	0.59	0.68	0.69	0.60	0.50	0.28	0.25	0.26	0.26	0.28	0.16	0.22	-0.10	-0.06	0.35	0.52
	R	0.12	0.06	0.04	0.53	0.31	0.39	0.34	0.46	0.48	0.36	0.25	0.08	0.06	0.07	0.07	0.08	0.02	0.05	0.01	0.00	0.12	0.28
	MBE	0.73	0.42	8.54	-1.83	-0.41	-0.89	1.66	-7.02	-2.73	2.77	5.55	-1.75	0.42	-2.25	-3.92	-1.57	-6.76	-0.93	-6.17	-0.94	0.73	-0.55
	RMSE	6.32	6.55	16.96	12.22	6.16	11.56	8.82	16.60	9.97	9.59	10.17	8.71	6.55	5.14	11.94	6.52	15.52	5.30	15.22	7.36	6.32	4.12
	S	0.80	0.43	0.83	0.71	0.70	0.59	0.68	0.42	0.55	0.73	1.03	0.18	0.43	0.21	0.12	0.23	0.05	0.30	-0.04	-0.06	0.80	0.76
KF2	NS	0.19	-0.07	0.02	0.09	0.14	-0.10	-0.05	-0.59	-0.31	-0.21	0.29	-0.67	-0.07	-0.55	-1.60	-0.85	-2.54	-0.45	-2.24	-0.94	0.19	0.24
	R2	0.44	0.28	0.18	0.68	0.50	0.54	0.50	0.57	0.48	0.52	0.57	0.44	0.28	0.18	0.37	0.21	0.13	0.15	-0.05	0.03	0.44	0.50
	R	0.19	0.08	0.03	0.46	0.25	0.29	0.25	0.32	0.23	0.27	0.32	0.19	0.08	0.03	0.14	0.04	0.02	0.02	0.00	0.00	0.19	0.25
	MBE	0.25	0.18	6.17	-5.00	-1.30	-3.71	-1.48	-8.81	-4.02	-1.63	1.82	-1.94	0.18	-2.44	-4.24	-1.70	-6.90	-1.96	-6.89	-2.00	0.25	-0.08
	RMSE	5.34	5.87	14.13	13.21	6.40	12.82	8.70	18.95	12.94	8.43	6.32	8.04	5.87	5.62	11.56	6.80	15.70	5.18	15.19	6.55	5.34	4.63
	S	0.90	0.42	0.65	0.53	0.61	0.46	0.48	0.34	0.39	0.42	0.86	0.31	0.42	0.16	0.19	0.17	0.04	0.16	-0.02	0.03	0.90	0.83
BMJ	NS	0.15	0.00	0.03	0.42	0.27	0.21	0.30	-0.20	0.07	0.31	0.13	-1.33	0.00	-0.53	-2.27	-0.81	-2.63	-0.24	-2.39	-0.81	0.15	0.26

GD	R2	0.40	0.29	0.19	0.73	0.57	0.61	0.61	0.68	0.64	0.62	0.42	0.41	0.29	0.28	0.28	0.22	0.12	0.23	-0.08	0.00	0.40	0.52
	R	0.16	0.08	0.04	0.53	0.32	0.37	0.37	0.46	0.41	0.38	0.17	0.17	0.08	0.08	0.08	0.05	0.01	0.05	0.01	0.00	0.16	0.27
	MBE	1.02	0.95	8.51	-2.33	-0.45	-1.12	0.79	-7.08	-2.86	1.74	4.42	-2.55	0.95	-2.40	-4.24	-1.46	-6.65	-1.29	-6.57	-1.53	1.02	-0.32
	RMSE	6.32	6.60	17.05	12.23	5.97	11.98	8.44	16.54	10.75	8.78	9.58	8.08	6.60	5.12	11.94	6.76	15.63	5.14	15.25	7.03	6.32	4.28
	S	0.94	0.50	0.80	0.70	0.71	0.60	0.70	0.44	0.53	0.71	0.80	0.23	0.50	0.23	0.12	0.18	0.04	0.29	-0.03	0.00	0.94	0.80
	NS	0.08	-0.03	0.03	0.35	0.25	0.13	0.31	-0.33	0.01	0.31	0.19	-1.19	-0.03	-0.68	-1.91	-0.84	-2.54	-0.41	-2.33	-0.90	0.19	0.24
	R2	0.31	0.27	0.21	0.69	0.55	0.58	0.61	0.64	0.63	0.61	0.48	0.36	0.27	0.21	0.34	0.21	0.12	0.18	-0.06	0.07	0.44	0.50
	R	0.10	0.07	0.04	0.48	0.31	0.33	0.37	0.41	0.40	0.37	0.23	0.13	0.07	0.04	0.11	0.04	0.02	0.03	0.00	0.00	0.19	0.25
	MBE	0.39	0.25	8.78	-1.95	-0.46	-0.47	0.95	-6.50	-2.85	2.04	4.95	-1.96	0.25	-2.43	-4.22	-1.66	-6.85	-1.88	-6.75	-1.88	0.29	0.01
	RMSE	6.58	6.67	16.99	12.81	6.18	12.40	8.52	16.97	10.76	9.15	9.86	8.33	6.67	5.25	11.67	6.82	15.70	5.05	15.13	6.42	5.38	4.68
S	0.74	0.46	0.85	0.66	0.71	0.56	0.71	0.41	0.50	0.73	0.98	0.23	0.46	0.17	0.16	0.17	0.04	0.20	-0.02	0.06	0.91	0.83	

Table 6: Temporal comparison (in terms of different continuous statistical indices) of different CPSs based WRF results with corresponding weather stations

CPSs	Indices	WRF Simulation days													
		1-Mar-99	2-Mar-99	3-Mar-99	4-Mar-99	5-Mar-99	6-Mar-99	7-Mar-99	8-Mar-99	9-Mar-99	10-Mar-99	11-Mar-99	12-Mar-99	13-Mar-99	14-Mar-99
KF1	NS	-0.50	0.02	-0.17	0.28	0.02	-0.52	0.18	-1.21	0.02	-0.75	-0.13	-0.44	0.02	-0.07

KF2	R2	0.09	0.57	0.46	0.69	0.51	0.49	0.51	0.66	0.33	0.33	0.08	0.54	0.30	0.10
	R	0.01	0.32	0.21	0.48	0.26	0.24	0.26	0.44	0.11	0.11	0.01	0.29	0.09	0.01
	MBE	-9.10	12.75	-3.02	5.43	-4.99	-14.57	9.57	-6.58	4.56	-3.68	0.00	-2.83	1.60	0.07
	RMSE	11.22	13.38	3.58	7.19	14.28	20.47	15.74	11.19	6.58	5.13	0.31	3.44	2.27	0.13
	S	0.01	2.33	0.30	1.01	0.51	0.24	0.92	0.22	0.57	0.11	0.18	0.10	0.59	0.22
	NS	-0.51	0.03	-0.26	0.35	-0.07	-0.67	0.29	-1.32	0.22	-0.57	-0.24	-0.44	0.02	-3.05
BMJ	R2	0.04	0.69	-0.13	0.76	0.54	0.37	0.61	0.71	0.71	0.42	0.13	0.59	0.30	-0.08
	R	0.00	0.48	0.02	0.58	0.29	0.14	0.37	0.50	0.51	0.18	0.02	0.35	0.09	0.01
	MBE	-9.17	11.95	-3.10	4.73	-6.56	-17.99	6.64	-7.33	-1.70	-4.62	-0.04	-3.02	1.43	0.00
	RMSE	11.29	12.32	5.78	6.09	13.67	23.73	11.85	11.89	2.64	5.84	0.23	3.63	2.08	0.05
	S	0.00	2.28	-0.25	1.00	0.47	0.08	0.94	0.17	0.63	0.06	0.20	0.06	0.56	-0.05
	NS	-0.50	0.02	-0.52	0.32	0.07	-0.52	0.18	-1.30	0.20	-0.71	-0.14	-0.46	-0.17	-0.16
	R2	0.09	0.57	-0.07	0.72	0.53	0.46	0.51	0.65	0.55	0.33	0.13	0.39	0.08	0.08
	R	0.01	0.33	0.00	0.52	0.28	0.21	0.26	0.43	0.30	0.11	0.02	0.15	0.01	0.01
	MBE	-9.10	12.69	-1.38	5.23	-5.05	-15.19	9.55	-6.54	2.23	-4.07	-0.01	-2.92	0.89	0.04
	RMSE	11.22	13.26	3.96	6.93	13.92	21.11	15.79	11.26	3.97	5.44	0.27	3.55	1.82	0.10
	S	0.01	2.24	-0.09	1.06	0.54	0.22	0.91	0.21	0.75	0.07	0.25	0.06	0.14	0.14

GD	NS	-0.50	0.02	-0.10	0.30	0.05	-0.59	0.19	-1.34	0.18	-0.73	-0.11	-0.46	0.02	-0.50
	R2	0.06	0.54	0.19	0.71	0.54	0.46	0.52	0.67	0.47	0.40	0.12	0.36	0.35	-0.09
	R	0.00	0.29	0.03	0.50	0.29	0.22	0.27	0.45	0.22	0.16	0.01	0.13	0.12	0.01
	MBE	-9.17	12.95	-3.18	5.48	-5.46	-14.92	9.26	-6.30	3.33	-3.81	-0.01	-2.93	0.77	0.03
	RMSE	11.29	13.51	4.70	7.19	13.76	20.88	15.67	11.06	7.01	5.18	0.30	3.56	1.47	0.09
	S	0.01	2.11	0.28	1.04	0.53	0.20	0.95	0.21	1.18	0.10	0.25	0.06	0.52	-0.12

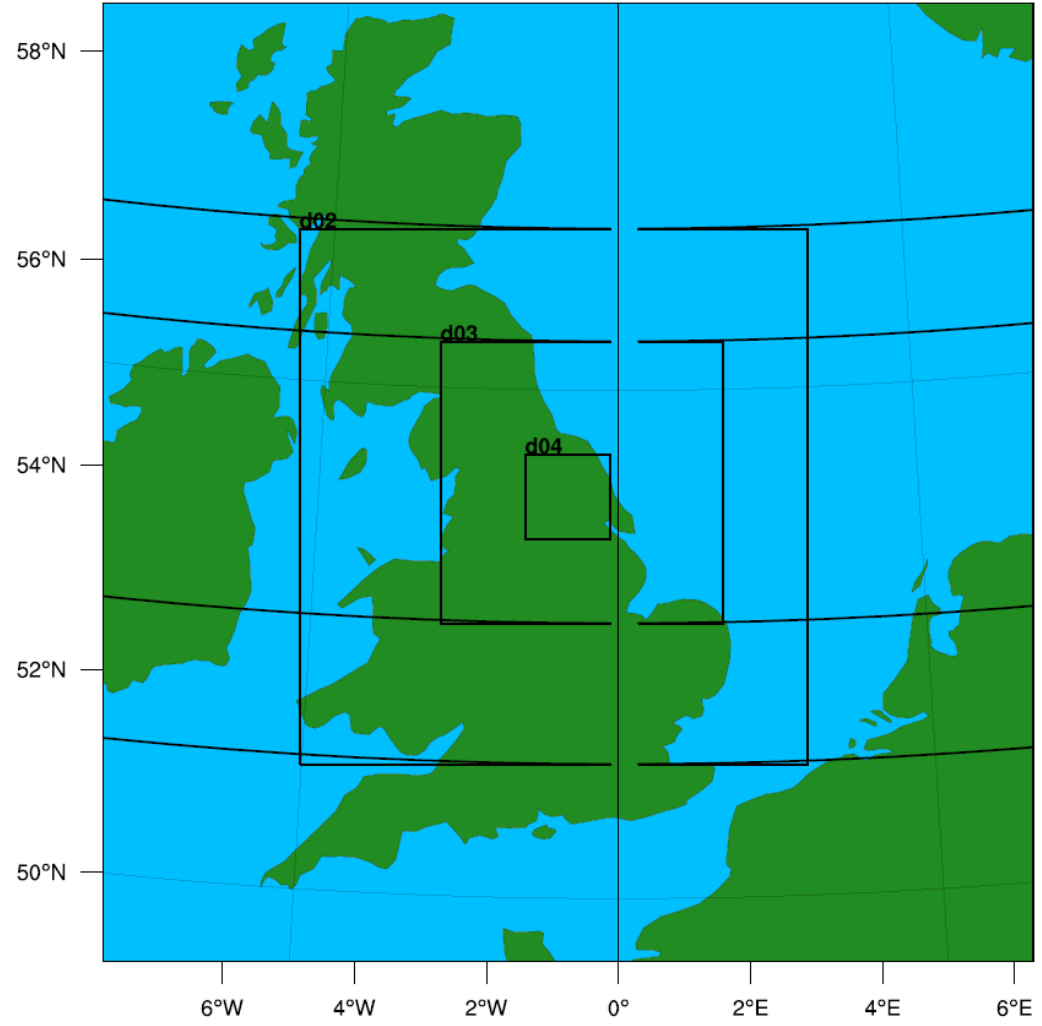


Figure 1 Dimensions of the nested domains for different model settings which are centred over the River Derwent catchment, Yorkshire-Humberside. d01, d02, d03 and d04 refer to the four domains (refer table 4 for details)

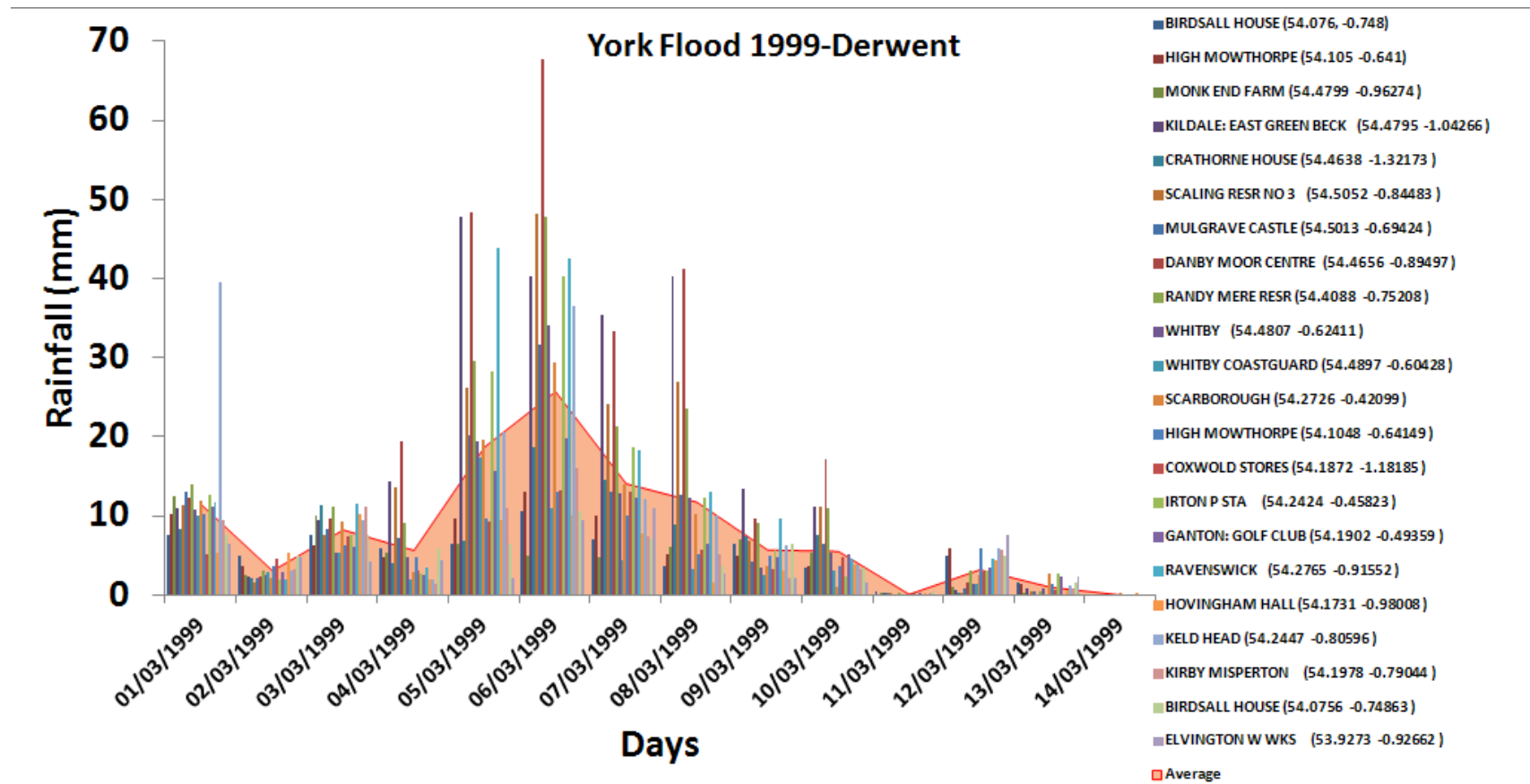


Figure 2: The observed rainfall during 1st March- 14th March 1999 from different stations at Derwent, Yorkshire [N.B. refer table 2 and figure 4 to for the locations of stations]

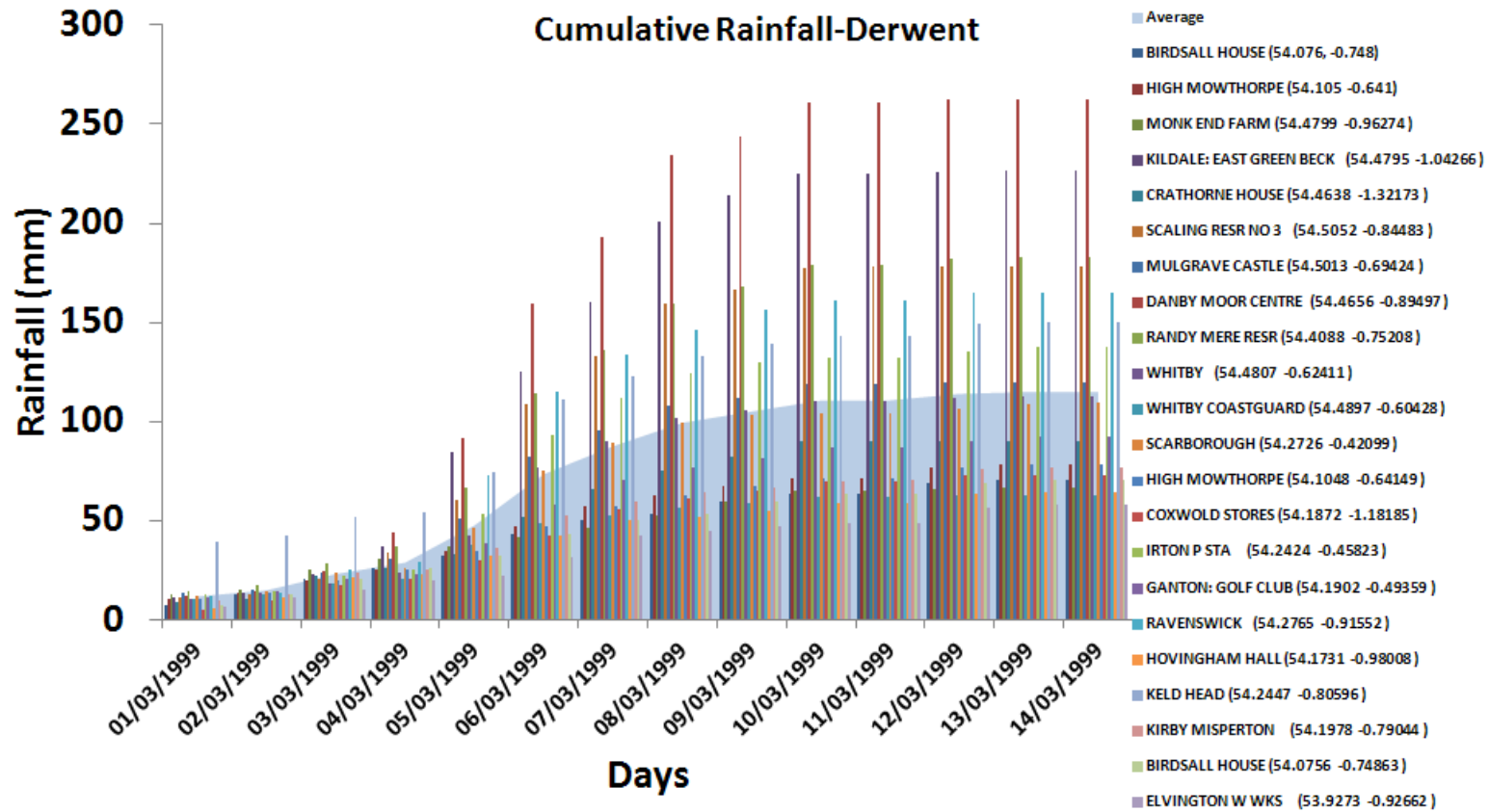
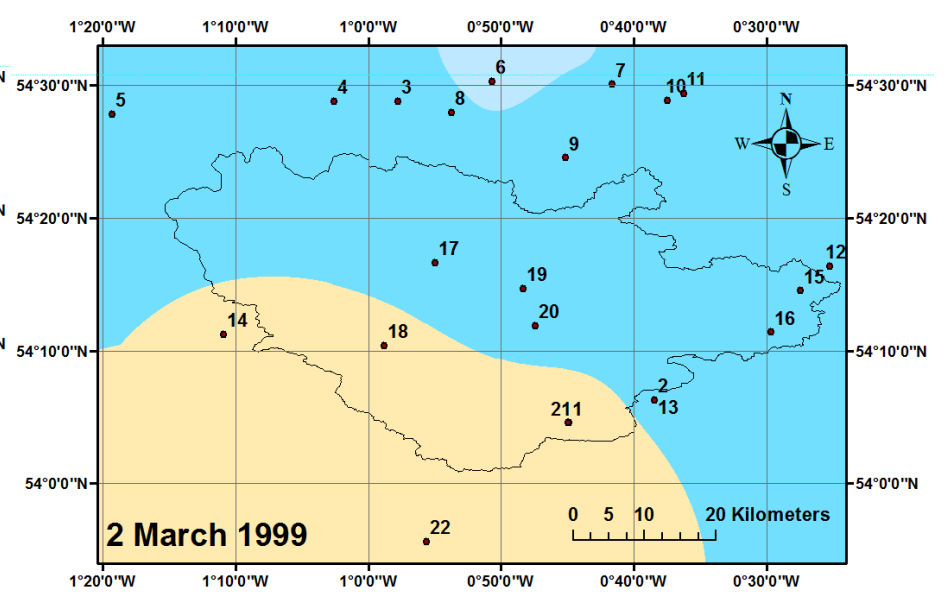
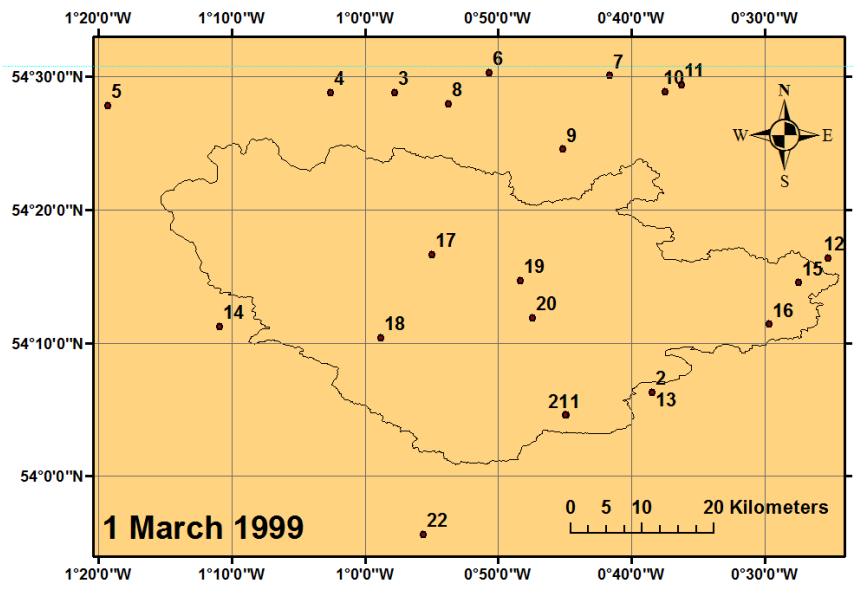
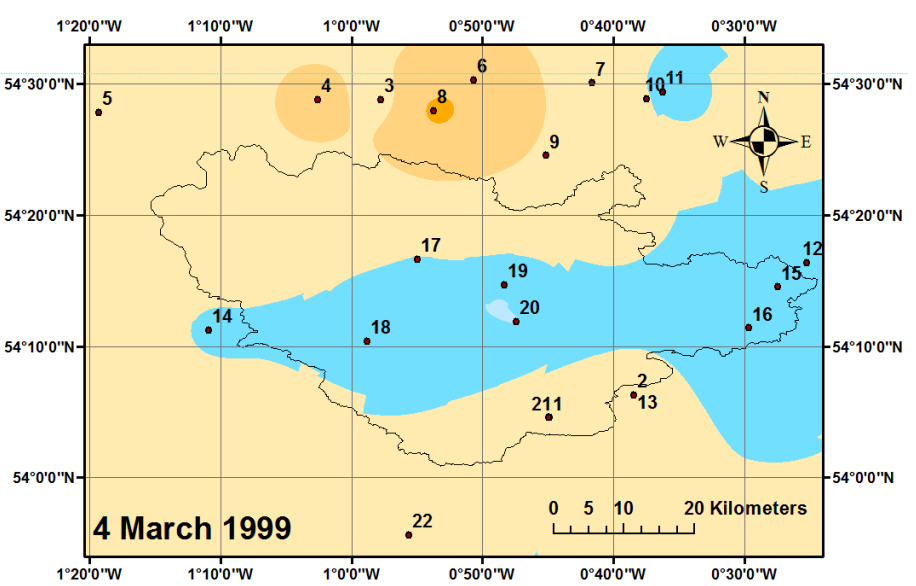
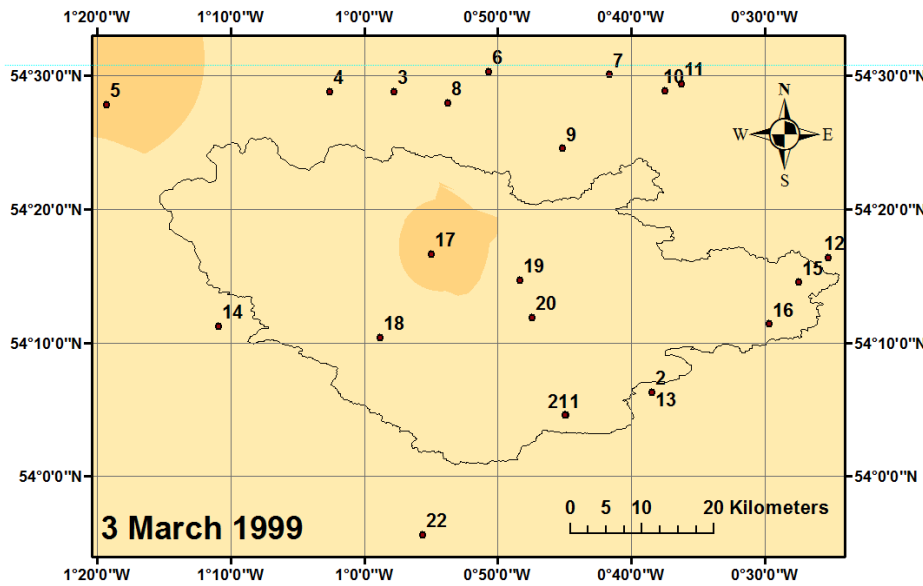
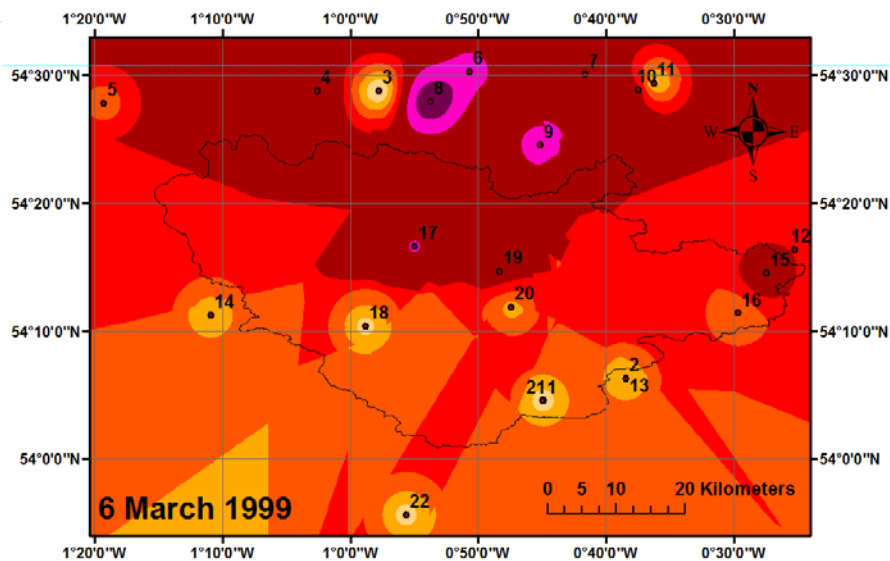
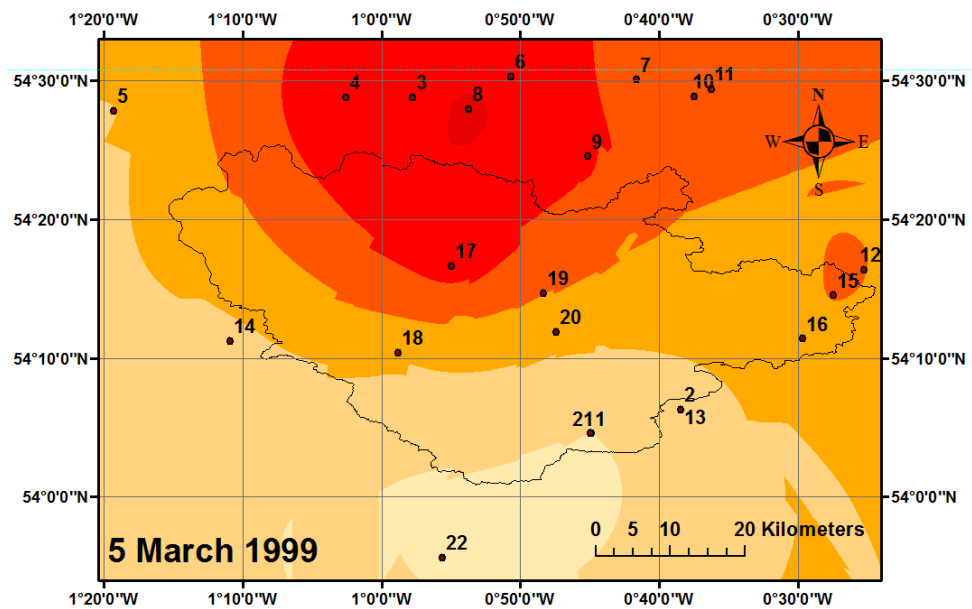
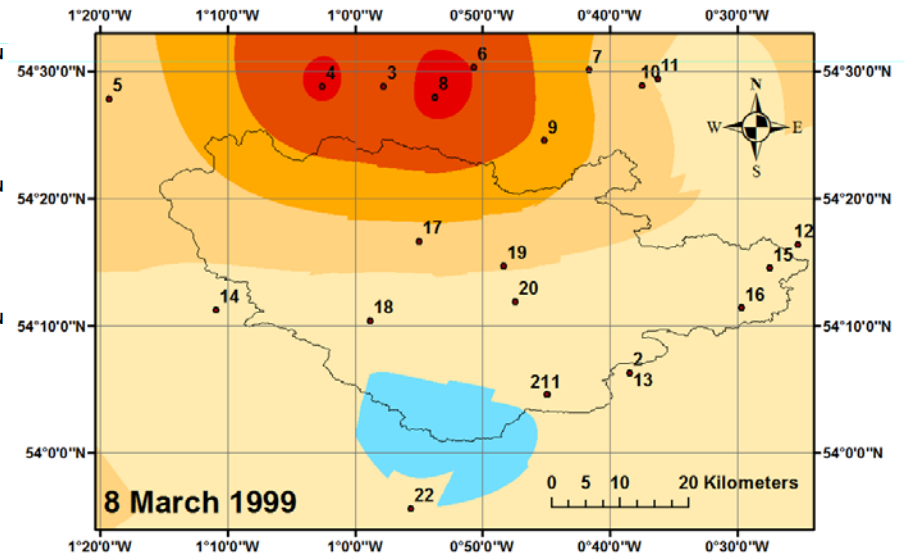
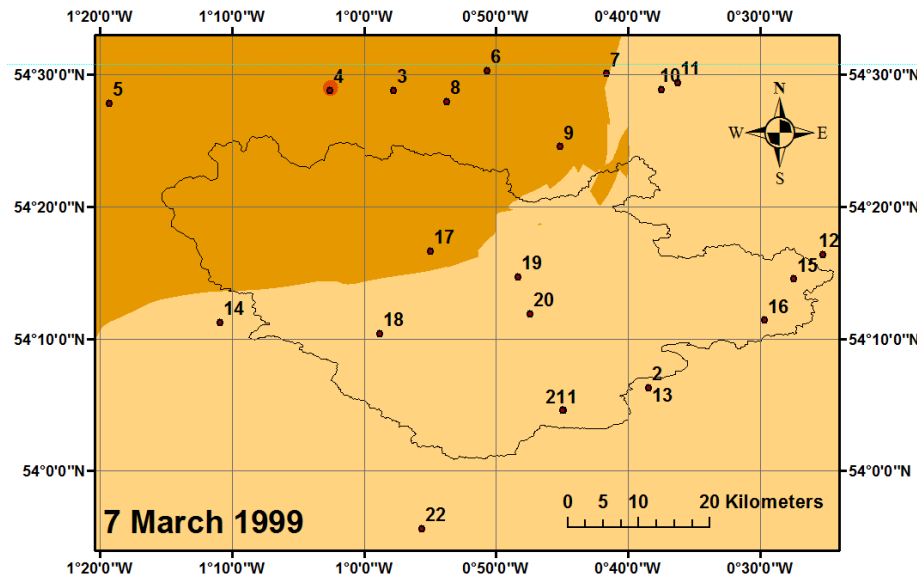


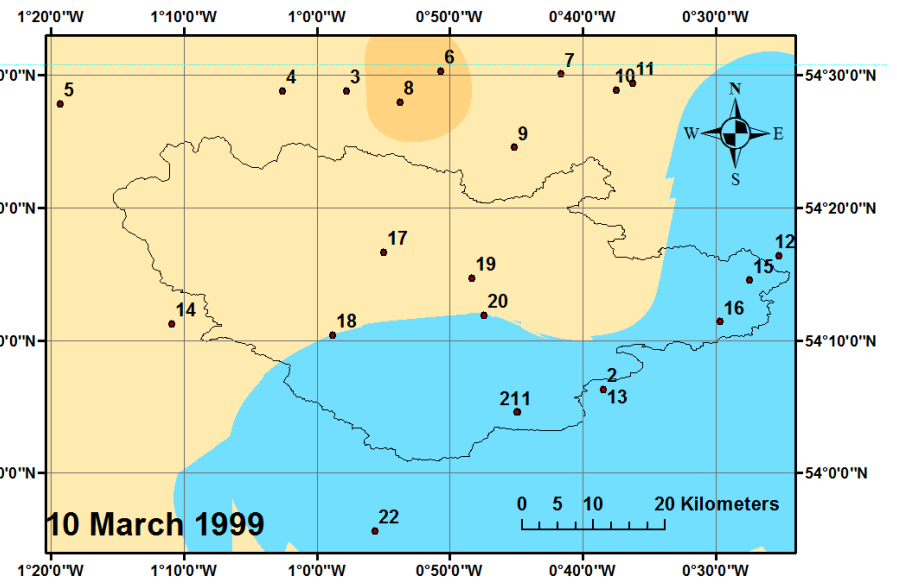
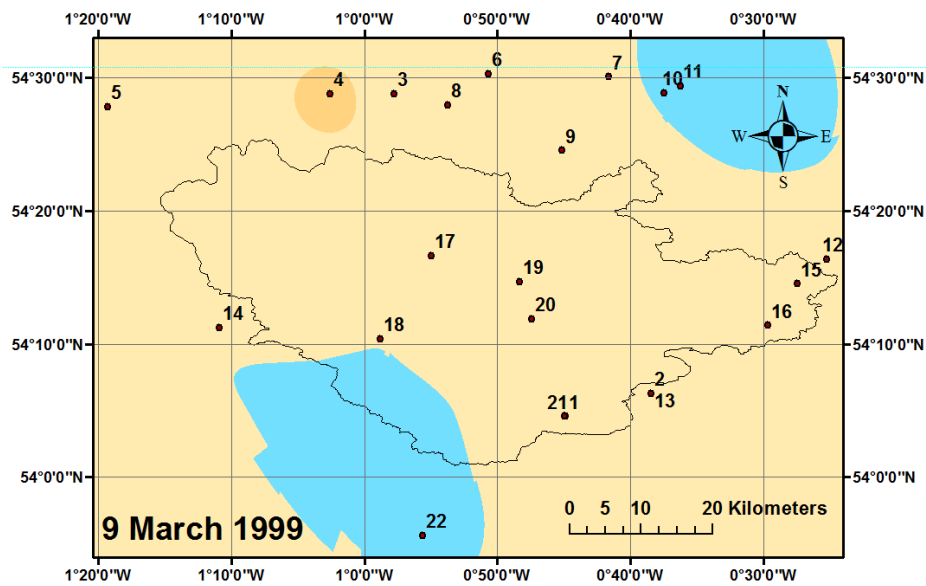
Figure 3: The accumulated rainfall during 1st March- 14th March 1999 from different stations at Derwent, Yorkshire [N.B. refer table 2 and figure 4 to for the locations of stations]

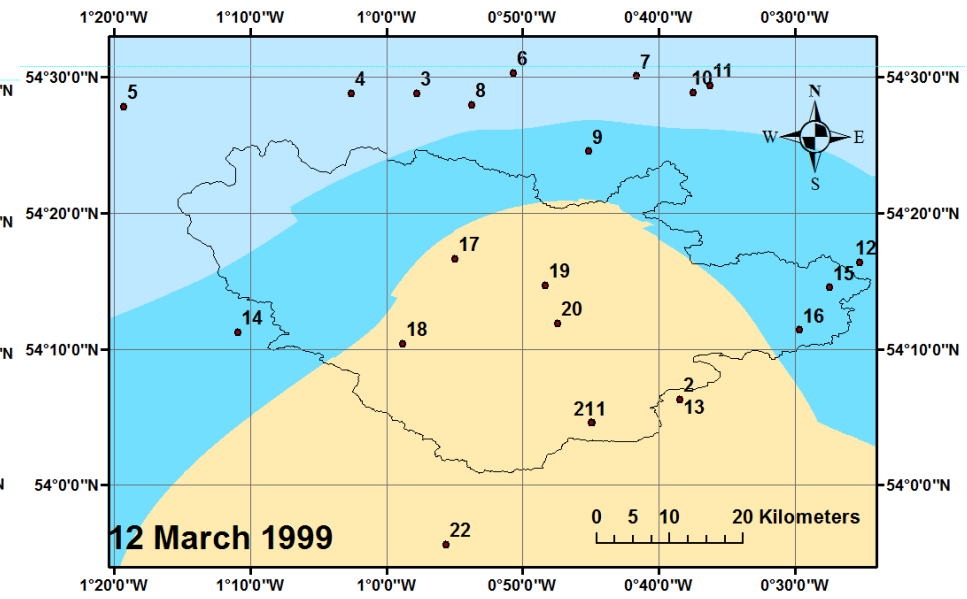
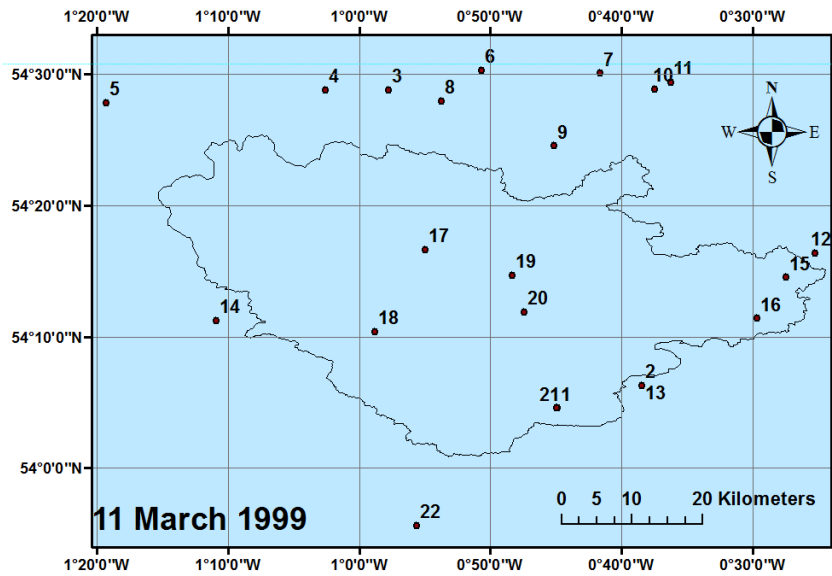


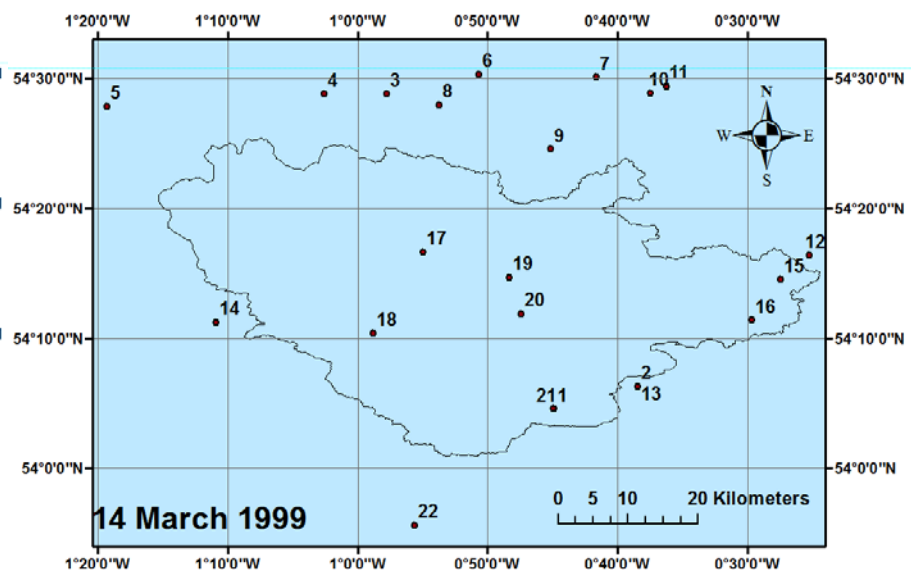
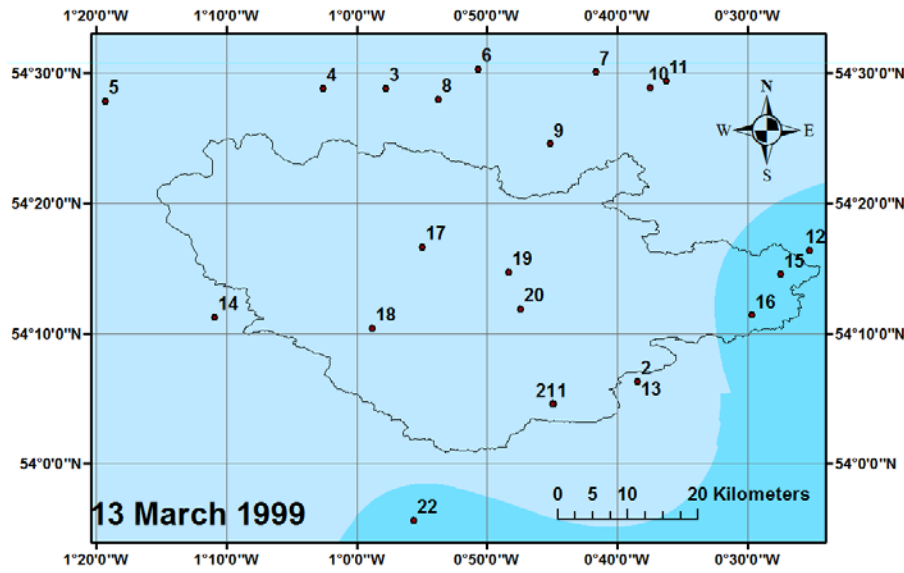












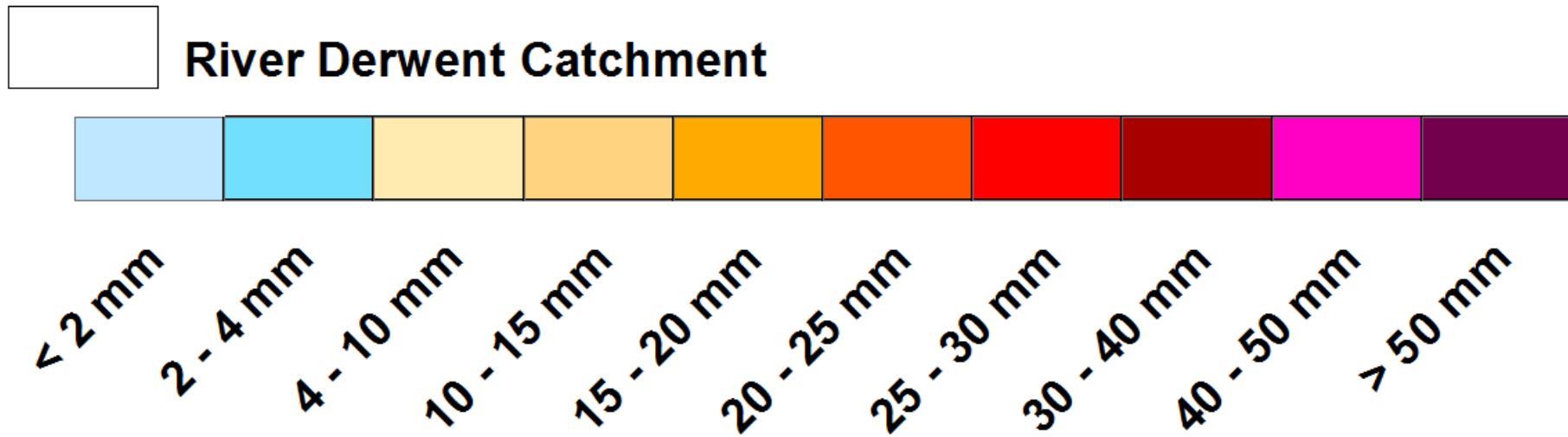


Figure 4: The spatial and temporal variation of precipitation during ‘York Flood – 1999’ period [N.B: the numbers are corresponding weather stations as mentioned in the table 2]

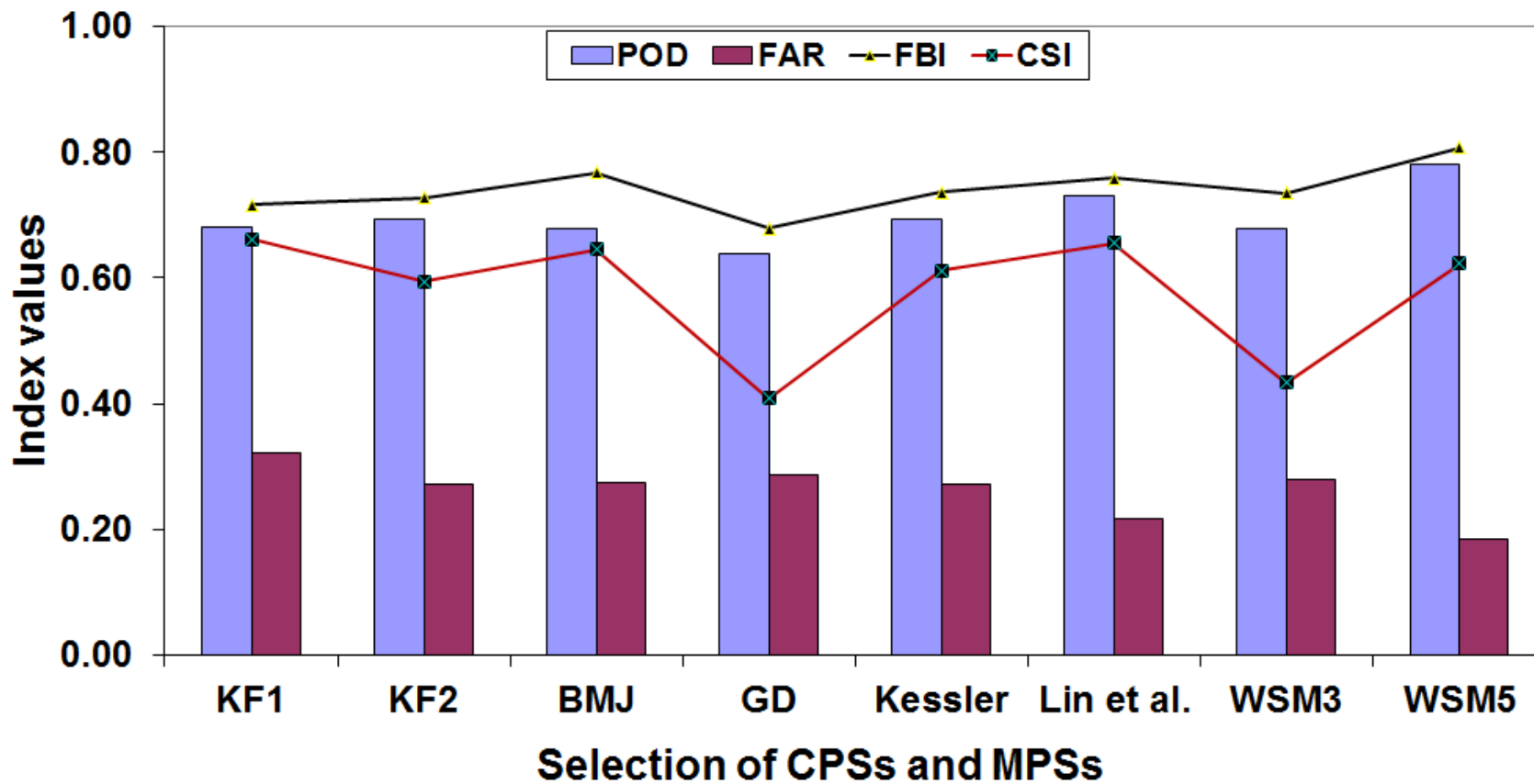


Figure 5: Spatial variation of categorical indices with selection of different CPSs and MPSs during York Flood - 1999

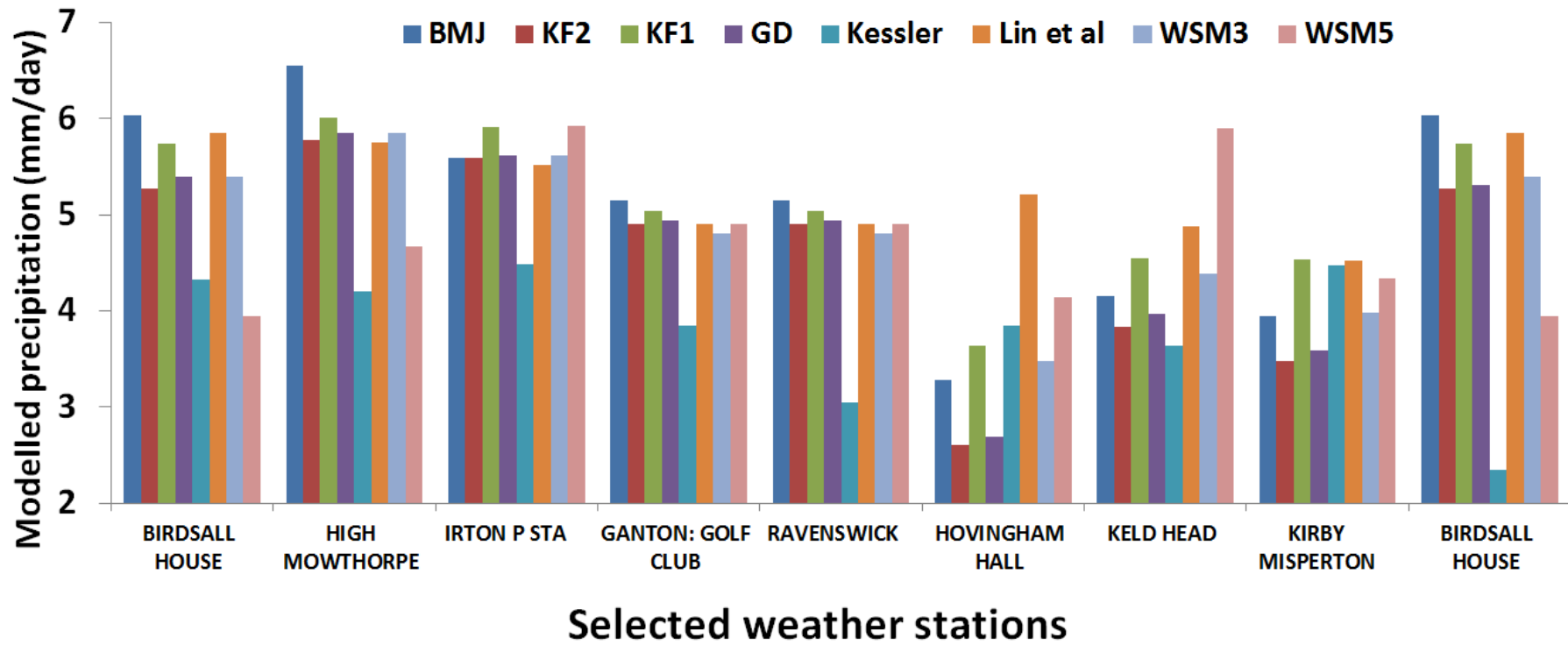


Figure 6: WRF simulated precipitation under different CPSs /MPSs and observed catchment precipitations during ‘York Flood -1999’ corresponding to different weather stations [daily average of 1st March- 14th March 1999]

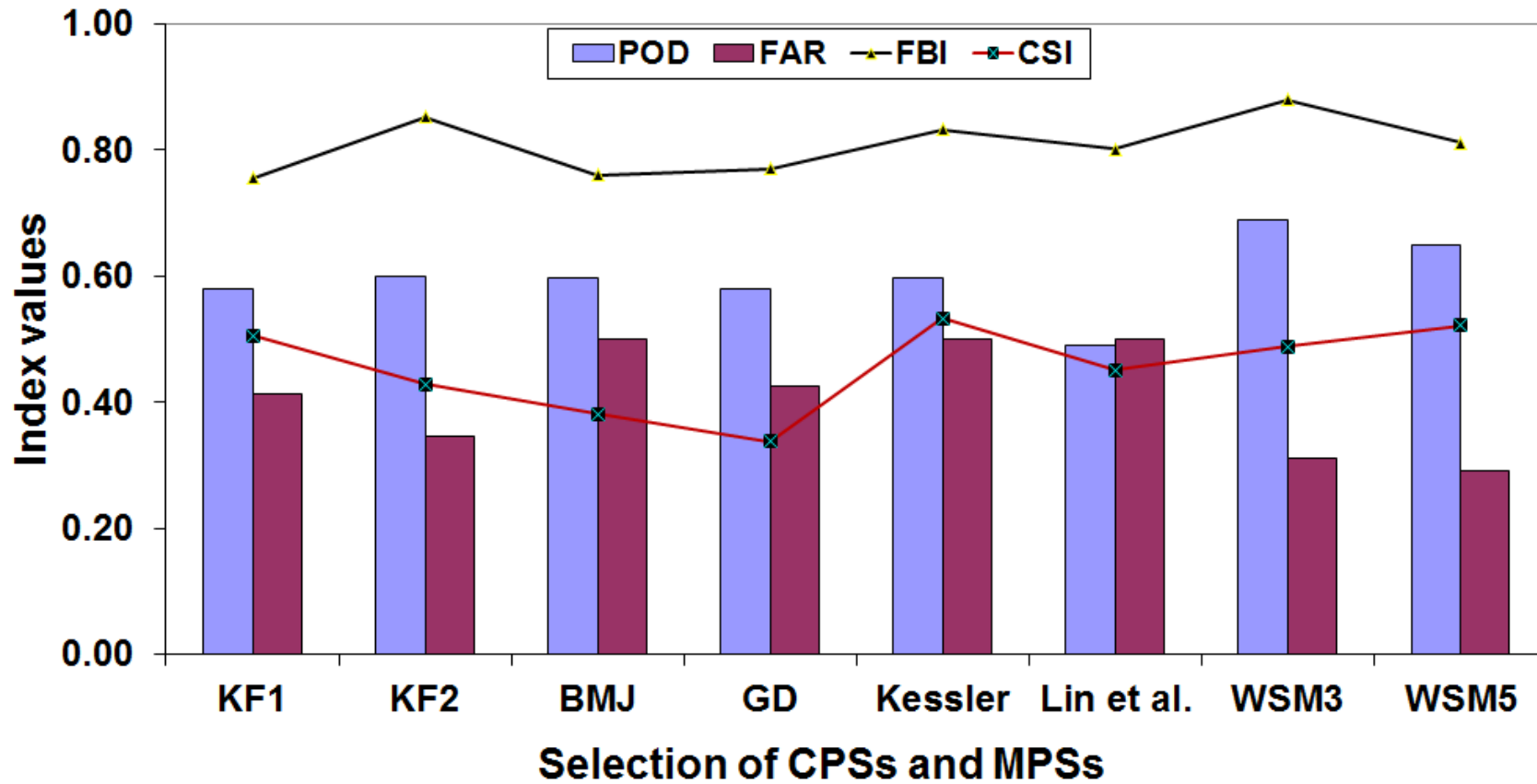


Figure 7: Temporal variation of categorical indices with selection of different CPSs and MPSs during York Flood- 1999

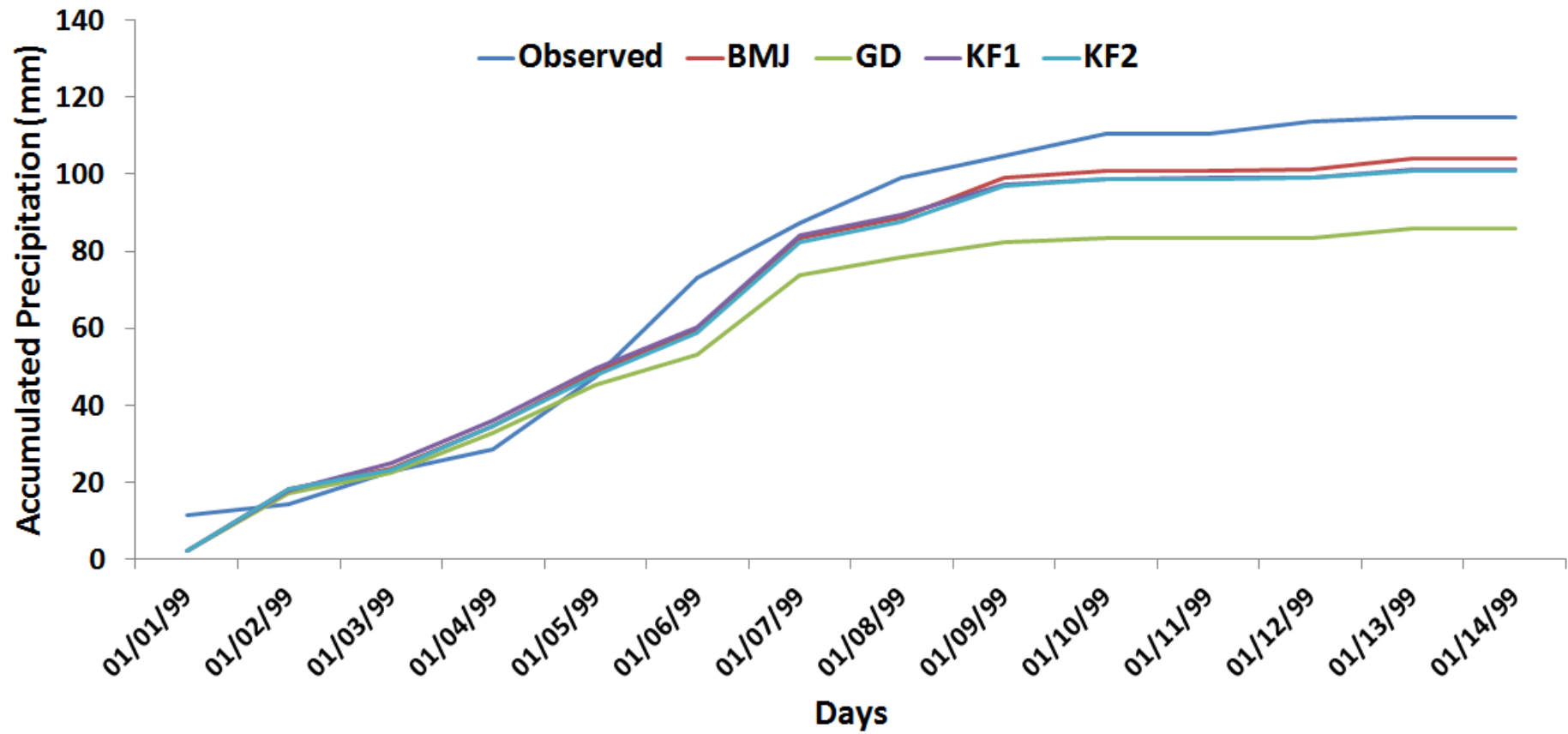


Figure 8: Cumulative variation of WRF predicted precipitation during 'York Flood - 1999' using different CPSs

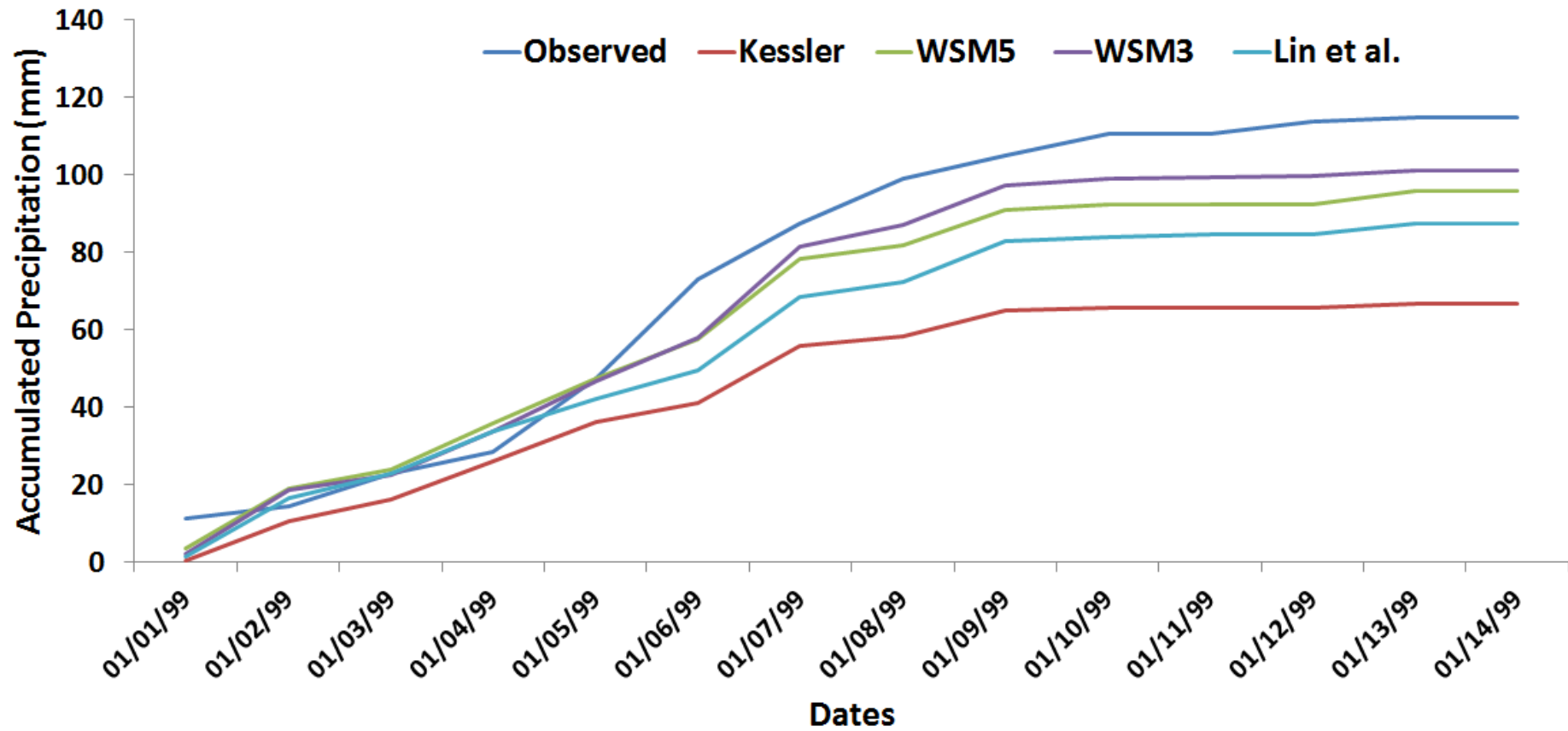
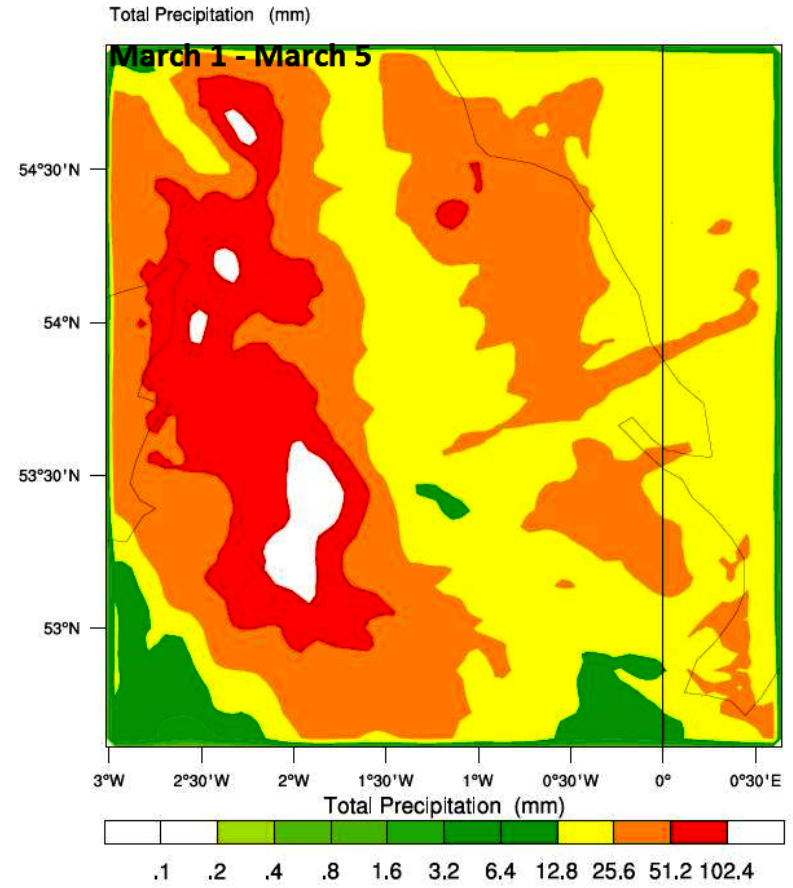
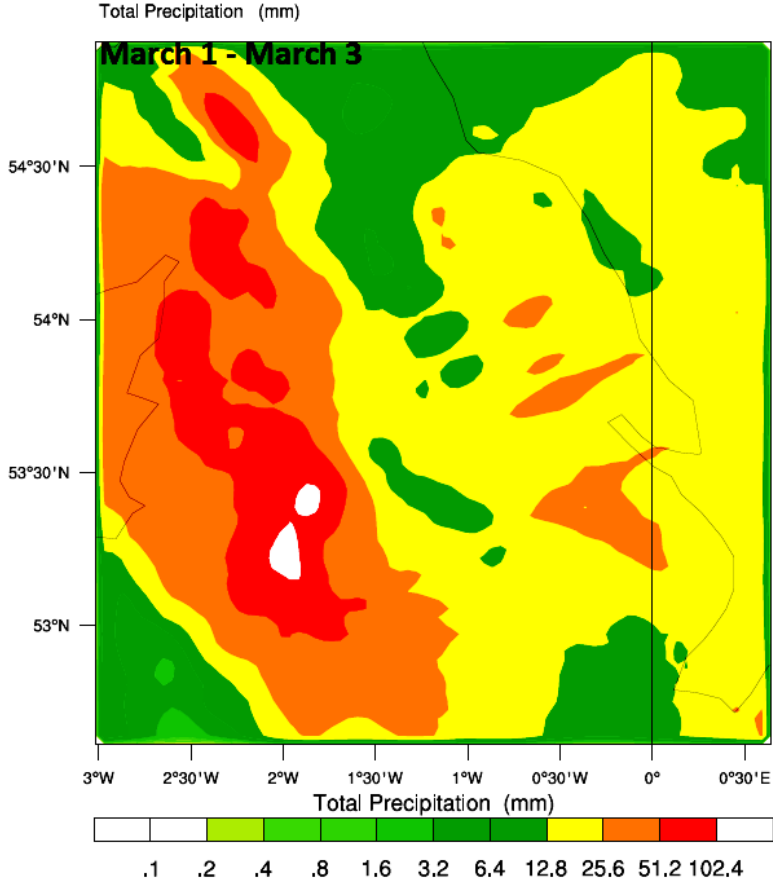
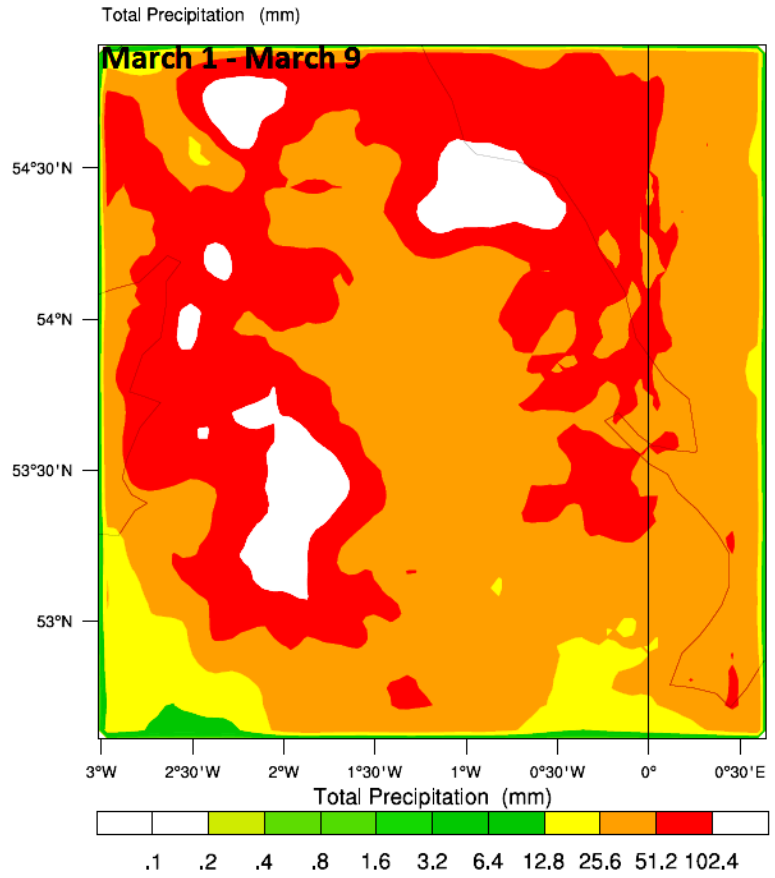
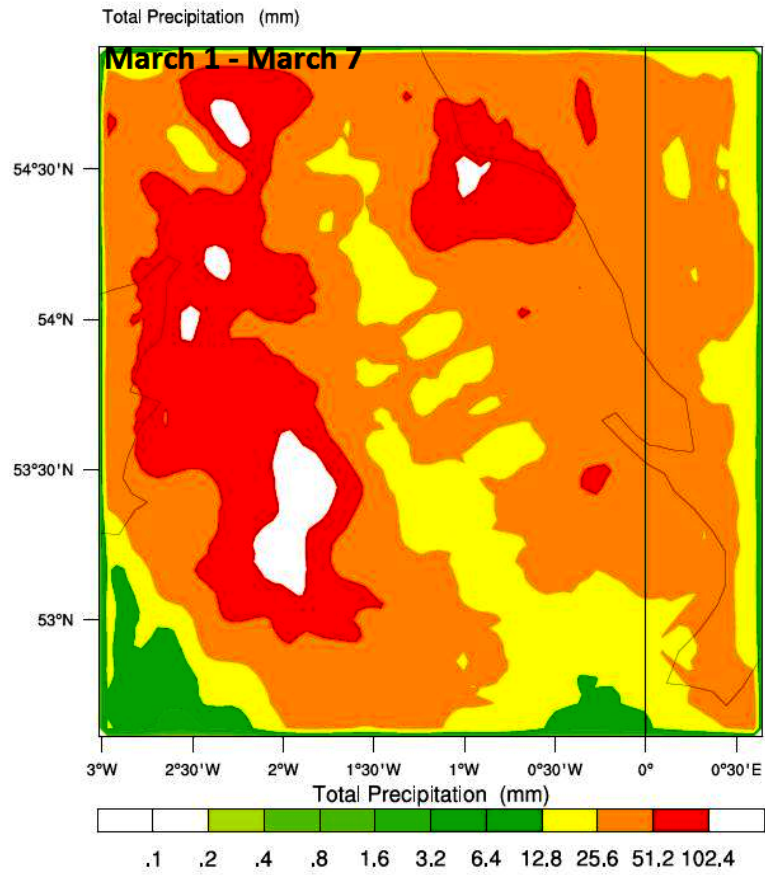
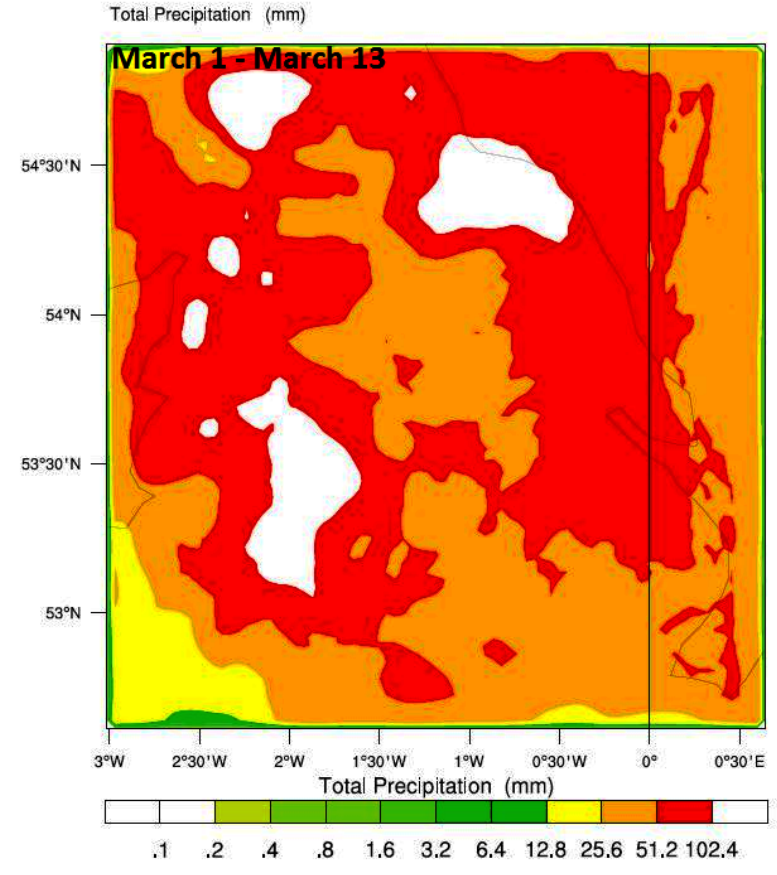
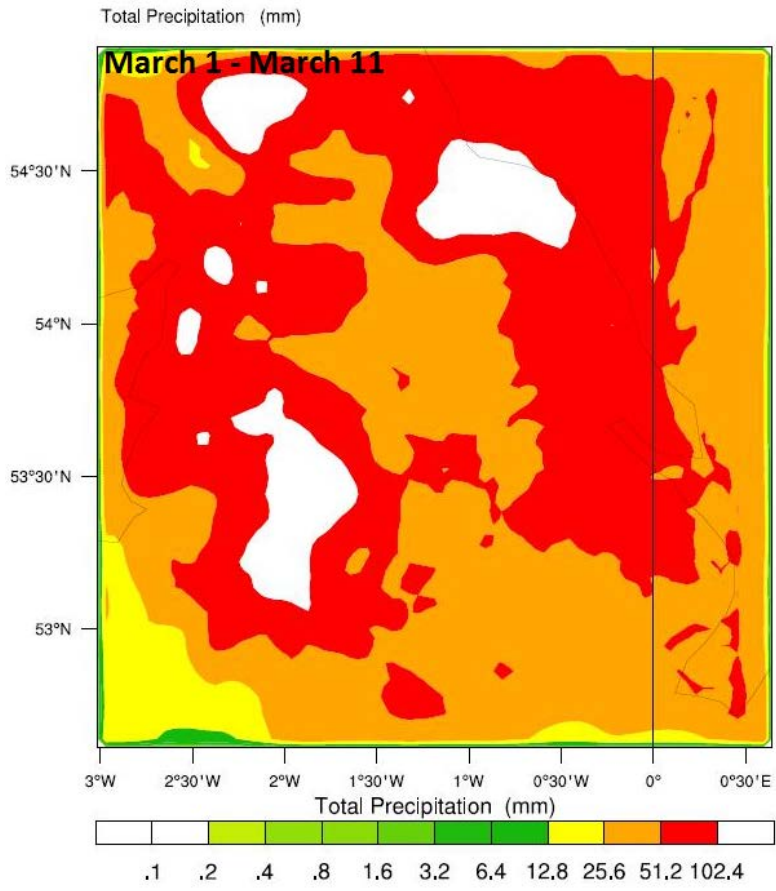


Figure 9: Cumulative variation of WRF predicted precipitation during ‘York Flood – 1999’ using different MPSs







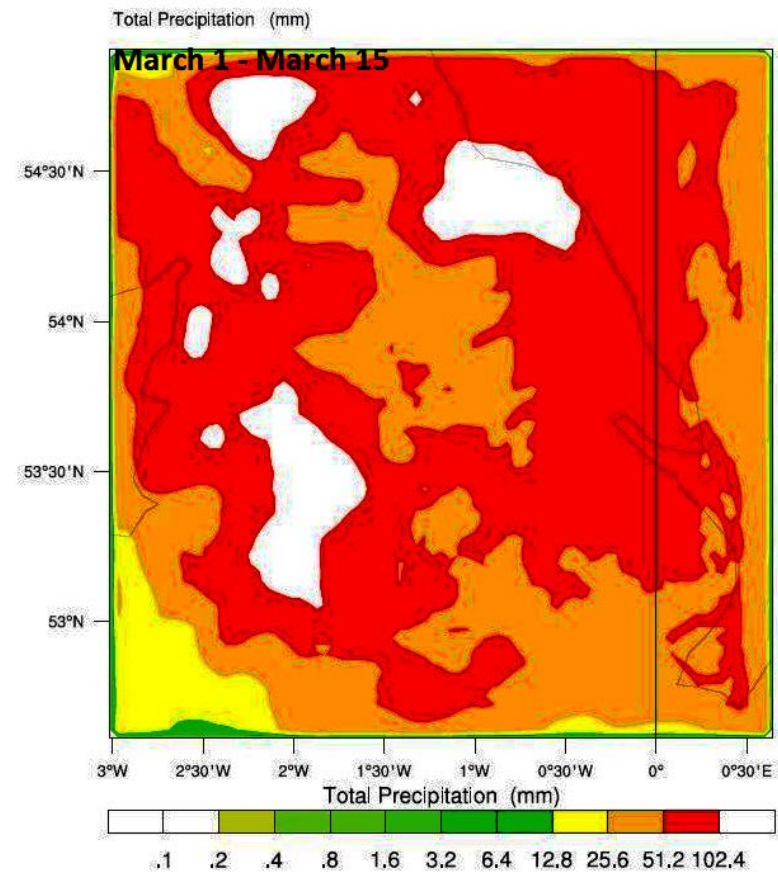


Figure 10: The accumulated precipitation results obtained from WRF with WRF SM3 and BMJ schemes from 1st March to 14th march

1999

